NBSIR 85-3168

Performance Requirements and Preliminary Design of A Boundary Layer Wind Tunnel Facility

R. D. Marshall

U.S. DEPARTMENT OF COMMERCE
National Bureau of Standards
National Engineering Laboratory
Center for Building Technology
Gaithersburg, MD 20899

May 1985

U.S. DEPARTMENT OF COMMERCE
NATIONAL BUREAU OF STANDARDS

NBSIR 85-3168

PERFORMANCE REQUIREMENTS AND PRELIMINARY DESIGN OF A BOUNDARY LAYER WIND TUNNEL FACILITY

R. D. Marshall

U.S. DEPARTMENT OF COMMERCE
National Bureau of Standards
National Engineering Laboratory
Center for Building Technology
Gaithersburg, MD 20899

May 1985

U.S. DEPARTMENT OF COMMERCE, Malcolm Baldrige, *Secretary*
NATIONAL BUREAU OF STANDARDS, Ernest Ambler, *Director*

TABLE OF CONTENTS

TABLE OF CONTENTS (Continued)

LIST OF TABLES

LIST OF FIGURES

ABSTRACT

This report describes performance characteristics and design details of a boundary layer wind tunnel for supporting research activities within the Center for Building Technology. Two preliminary designs, the first consisting of a conventional closed-circuit scheme in an over/under configuration and the second consisting of an open-circuit scheme with a "pusher" or "blow-down" configuration, are addressed. Both tunnels incorporate a three-dimensional contraction with a 3.2:1 contraction ratio and a test section having a width of 10 ft (3.048 m) and a height of 6 ft (1.829 m). The test section length allows for the natural development of rough-wall boundary layers of sufficient depth for 1:500 scale simulations of the atmospheric boundary layer. To ensure stable operation over the design speed range of 1 to 75 fps (0.30 to 22.86 m/s), both variable pitch and variable speed fan control will be required.

Key Words: Aerodynamics; boundary layers; buildings; modeling; wind engineering; wind tunnels.

DESIGN OVERVIEW

This report addresses performance requirements and the preliminary design of a boundary layer wind tunnel facility for supporting research activities that involve the physical modeling of the planetary boundary layer and its effects on engineering structures. It is anticipated that the wind tunnel will be supported and operated under the concept of a regional research facility. Thus, in addition to supporting selected research activities within the Center for Building Technology, the facility will be utilized by universities, research establishments and other Federal agencies having a common interest in wind engineering.

Potential research applications include, but are not limited to, the following topics.

- Wind forces on buildings and other structures
- Aeroelastic phenomena
- Natural and forced ventilation of buildings
- Infiltration/exfiltration
- Thermal performance of buildings
- Modeling and measurement techniques
- Instrument development
- Interpretation and extension of full-scale measurements
- Related topics such as turbulent diffusion, smoke migration and drifting snow.

In addition to those measurements required for the characterization of turbulent flows, the supporting measurement capability will include pressure, force, moment, torque, displacement, acceleration and temperature. Certain studies may require capabilities for flow visualization, the measurement of surface shear stress, or the measurement of tracer gas concentrations. In this design effort the emphasis has been placed on aerodynamic issues. Wind tunnel instrumentation and structural design issues will be addressed elsewhere.

Although a thermal modeling capability would be useful, the requirements for such a capability within the Center for Building Technology have not been developed to the point where they can be put in the form of wind tunnel design criteria. Two basic tunnel designs have been considered; the first employing a closed-circuit arrangement (figure 1) and the second consisting of an open-circuit arrangement (figure 12). Both designs can meet the performance requirements for speed range, flow quality and physical size of the test section. However, only the closed-circuit design is adaptable to thermal modeling. Construction costs for the open-circuit design are expected to be substantially less than those associated with the closed-circuit design.

The laboratory space available for tunnel construction is 29 x 132 ft (8.84 x 40.23 m) in plan and the clear headroom is 21 ft (6.40 m). Allowing for a modest contraction ratio and adequate working space along the sides and end of the tunnel, the test section dimensions are limited to width = 10 ft (3.048 m), height = 6 ft (1.829 m) and length ≈ 60 ft (18.288 m). The range of operating speeds is dictated by similarity requirements; the Froude number

criterion indicating a minimum speed of approximately 1 fps (0.03 m/s) and the Reynolds number criterion indicating an upper limit of from 70 to 80 fps (21.34 to 24.38 m/s) to achieve critical values of Reynolds number. The intensity of turbulence and nonuniformity of the flow entering the test section do not place significant constraints on the tunnel design and nominal values of 0.5 and $\pm$ 1 percent have been adopted as performance criteria for intensity of turbulence and velocity nonuniformity, respectively.

Scale ratios of from 1:50 to 1:500 constitute a practical limit on partial-depth modeling of the planetary boundary layer on one hand and the construction of detailed building models on the other hand. Blockage effects due to boundary layer development and the presence of models in the test section require that the ceiling height be adjustable in order to maintain a zero pressure gradient along the length of the test section. Wide-angle diffusers have been employed in both designs to allow adequate length in the test section for natural development of a turbulent boundary layer. Use of these diffusers entails significant head losses with a correspondingly low tunnel energy ratio. The estimated energy ratio for the closed-circuit tunnel is 0.53, compared with 0.39 for the open-circuit design.

Both designs require a variable speed drive motor which can be of the induction type with frequency regulation or of the direct current type with voltage regulation. The closed-circuit design incorporates an axial flow fan with selectable pitch blades. Pitch selection is essential for stable tunnel operation at the lower end of the design speed range. The open-circuit design utilizes a double-wheel, double-inlet centrifugal fan with backward-curved blades. In addition to a variable speed drive, this fan will require adjustable inlet vanes to ensure stable operation at low speeds.

Basic dimensions of the two designs and their performance characteristics are summarized in the following table.

SUMMARY OF BASIC DIMENSIONS AND PERFORMANCE CHARACTERISTICS
FOR TWO TUNNEL DESIGNS

Feature	Closed-Circuit Tunnel	Open-Circuit Tunnel
General arrangement	Over/under	Blowdown or "pusher"
Overall length	117 ft	111 ft
Test section dimensions		
Width	10 ft	10 ft
Height	6 ft	6 ft
Length	55 ft	50 ft
Speed range	1 to 75 fps	1 to 75 fps
Speed deviation across test section	$\pm$ 1 percent	$\pm$ 1 percent
Turbulence intensity	0.5 percent	0.5 percent
Flow conditioning	Honeycomb/screen	Honeycomb/screen
Contraction ratio	3.2:1	3.2:1
Fan type	Axial flow	Centrifugal; double inlet, backward-bladed
Blade or wheel diameter	96 inches	98 inches
Power	150 hp	200 hp
Speed regulation	Variable speed drive and selectable pitch blades	Variable speed drive and vaned inlet
Energy ratio	0.53	0.39

1 ft = 0.3048 m

1. INTRODUCTION

This report describes the development of performance criteria and the preliminary design of a closed-circuit boundary layer wind tunnel and an alternate open-circuit tunnel for supporting selected research activities within the Center for Building Technology. The design effort described herein addresses aerodynamic considerations and power requirements only. Detailed structural design and instrumentation requirements will be addressed elsewhere.

The major function of a boundary layer wind tunnel facility will be to support wind engineering research activities. It is anticipated that wind tunnel investigations will range from studies of the aeroelastic behavior of bluff bodies placed in smooth flow to assessments of the dynamic response of complex engineering structures immersed in highly turbulent boundary layers. The development of thick, turbulent boundary layers as representations of the atmospheric boundary layer will also be an area of study.

In addition to measurements normally required to characterize the flow in a wind tunnel test section, measurements of the steady and fluctuating components of wind-induced pressures, forces, moments and displacements will be carried out. Improved instrumentation and measurement techniques are expected to be major subjects for study. These activities will support the traditional role of NBS/CBT in measurement technology and assurance.

Other areas of research within the Center for Building Technology that are expected to benefit from a boundary layer wind tunnel facility include natural and forced ventilation, infiltration/exfiltration, building heat transfer, drifting snow and diffusion of pollutants. Potential applications outside the Center for Building Technology include studies of smoke movement in buildings by the Center for Fire Research and building research needs of other Federal agencies for which the simulation of the atmospheric boundary layer is a requirement.

2. PERFORMANCE REQUIREMENTS AND DESIGN CONSTRAINTS

2.1 GENERAL

The following sections of this report identify the performance characteristics that a boundary layer wind tunnel should possess in order to meet the needs of the anticipated research applications. Limitations of cost and available laboratory space are also considered in arriving at a set of criteria for the aerodynamic design of a boundary layer wind tunnel facility.

2.2 SPEED RANGE

There are a number of factors that influence the choice of wind tunnel speed range which ultimately involves a compromise between similarity requirements and constraints such as available space, size of facility and cost. Considering first the investigation of wind forces acting on buildings and similar structures,

which will be the primary function of the facility, the basis for similitude should be the Reynolds number

$$R_e = \frac{Ud}{\nu} \tag{1}$$

where U is the wind speed, d is a characteristic dimension (such as breadth or diameter) of the structure and ν is the kinematic viscosity. Taking 1:50 to 1:500 as a practical range of geometric scale ratios for modeling buildings and other structures, Reynolds number equality would require tunnel speeds of from 50 to 500 times the full-scale speeds. Fortunately, the Reynolds number criterion usually is not important in the case of sharp-edged bodies for which the points of flow separation tend to be fixed. However, this relaxation of the Reynolds number criterion cannot, in general, be extended to bodies with curved surfaces, e.g., domes and circular cylinders.

With regard to studies involving isolated bluff bodies such as circular cylinders, the facility should be capable of attaining critical Reynolds numbers as this flow regime is encountered in many practical situations and is basic to the understanding of fluid/structure interaction. Critical Reynolds numbers for a circular cylinder range from about 2×10^5 to 6×10^6, depending on the incident turbulence and the surface roughness [1]. By choosing a sufficiently large cylinder diameter, this range of Reynolds number could be attained at modest tunnel speeds. However, as will be discussed later, the effects of blockage place rather severe limitations on the size of models that can be tested in an enclosed jet and a cylinder diameter of 0.5 ft (152 mm) can be taken as a reasonable upper bound. The corresponding range of tunnel speeds required to attain critical Reynolds numbers is approximately 70 to 200 fps (21.34 to 60.96 m/s). Since the power demand is proportional to the cube of the speed, there is little incentive to set the upper bound on speed much above the lower end of this range.

Two other dimensionless numbers that can be of importance in the modeling of certain engineering structures are the reduced velocity

$$U_r = \frac{U}{n_o d} \tag{2}$$

and the Froude number

$$F_r = \frac{U}{\sqrt{gd}} \tag{3}$$

were n_o is the frequency associated with a particular mode shape of the structure and g is the gravitational constant. Since the frequency, n_o, can be altered by changing the construction of the model, the reduced velocity is not a major consideration in establishing the speed range of the tunnel.

However, Froude number equality requires relatively low tunnel speeds; approximately 4 percent of the prototype speed for a scale ratio of 1:500. It is not unusual for certain full-scale structures to exhibit significant dynamic response at speeds of 20 mph (8.94 m/s) or less. A 1:500 scale simulation modeled on the basis of the Froude number will require stable tunnel operation at speeds as low as 1 fps (0.30 m/s).

Based on the factors discussed in the preceding paragraphs, a speed range of 1 to 80 fps (0.30 to 24.38 m/s) is a reasonable choice for the investigation of wind forces on buildings and other structures. This precludes the modeling of most engineering structures on the basis of Reynolds number equality, a problem that is common to practically all low speed boundary layer wind tunnels.

Similitude requirements for other modeling applications such as drifting snow and forced convection place certain demands on tunnel speed, but these demands tend to fall within the range required for the investigation of wind forces and structural response. Modeling laws for many non-structural applications can be found in references 2 and 3.

2.3 FLOW QUALITY

Flow quality includes background turbulence and uniformity of the flow entering the test section. Neither of these factors poses a serious limitation on studies conducted in thick, turbulent boundary layers. However, background turbulence and flow uniformity can be critical when conducting studies in smooth flow, the aeroelasticity of bluff bodies being one example.

Performance characteristics for a number of low-speed wind tunnels specifically designed for industrial aerodynamics applications are listed in reference 4. These characteristics suggest that turbulence intensities of the order of 0.5 percent and nonuniformity of the flow of about $\pm$ 1 percent on entry to the test section can be achieved using a modest number ($\overline{2}$ or 3) of damping screens and contraction ratios (ratio of inlet area to outlet area) that range from 3:1 to 8:1. Since these levels of turbulence intensity and nonuniformity of flow present no serious limitations on the research applications envisioned for the tunnel, they will be adopted as design criteria.

2.4 SIZE OF TEST SECTION

In order to set limits on the size of the test section, it is necessary to establish the model scale and the amount of blockage that can be tolerated. Issues that relate to the selection of model scale in the modeling of engineering structures and atmospheric boundary layers have been assessed by Vickery [5] and by Teunissen [6]. For large engineering structures and full-depth simulations of the atmospheric boundary layer, Vickery concludes that the linear scale should not be smaller than about 1:500 and that the practical consideration of being able to work in the test section while standing up sets the lower limit on height of the test section at about 6 ft. (1.83 m).

The minimum width of the test section can be related to the diameter of the turntable required for mounting models of adjacent structures and significant terrain features. Ideally, the radius of the turntable should be as large as the distance over which wake effects produced by objects surrounding the test structure are likely to persist. Britter [7] has addressed this question and suggests that the maximum velocity deficit, ΔU_{MAX}, behind a bluff body immersed in a turbulent boundary layer decays according to the relationship

$$\frac{\Delta U_{MAX}}{U_h} \simeq \frac{A}{(X/h)^{3/2}} \tag{4}$$

where ΔU is the difference between the approach flow velocity and the wake velocity, U_h is the approach flow velocity at the height h of the bluff body, A is a function of the body geometry and boundary layer depth, and X is the distance downstream of the body. Measurements carried out on models placed in a turbulent boundary layer suggest that $A \simeq 2.5$ for typical building shapes. Assuming a prismatic building 100 x 100 ft (30.48 x 30.48 m) in plan, 400 ft (122 m) high and modeled at a linear scale of 1:500, approximately 7 ft (2.13 m) would be required for the velocity deficit to decay to an acceptable level of approximately 10 percent of the approach flow velocity. This implies a minimum turntable diameter of about 14 ft (4.27 m) and a slightly larger test section width. The 14 ft (4.27 m) requirement would enable a complete model of surrounding bluff bodies to be mounted conveniently on the turntable. However, this is a convenience rather than a strict requirement for the modeling of significant surrounding features of a given full-scale site.

Other factors that influence choice of test section width are the effects of blockage, available laboratory floor space, capacity of the fan and required power. With regard to blockage effects, a solid blockage of from 3 to 5 percent of the test section area should be considered as an upper limit [5,8] if significant distortions in surface pressures and drag forces are to be avoided. Taking as the limiting case a circular cylinder spanning the test section vertically, a test section width of 10 ft (3.048 m) would be required to satisfy the 5 percent blockage limit for a cylinder diameter of 0.5 ft (152 mm). As was noted earlier, this is the diameter required to attain critical Reynolds numbers when operating at maximum tunnel speed. Also, a width in excess of 10 ft (3.048 m) would seriously limit the laboratory working space available along the sides of the test section. Finally, a tunnel speed of 80 fps (24.38 m/s) and test section dimensions of W = 10 ft (3.048 m) and H = 6 ft (1.829 m) will require a flow rate of 288,000 cfm (136 m^3/s). Axial flow fans with capacities up to about 300,000 cfm (142 m^3/s) and of standard design are readily available while fans of larger capacity tend to be special designs with a correspondingly higher cost. For these reasons, 10 ft (3.048 m) is considered to be a reasonable choice for width of the test section.

The length of the test section is dictated by the distance required to develop a turbulent boundary layer of sufficient thickness to simulate atmospheric boundary layers. Assuming a full-scale thickness of approximately 1500 ft (457 m) the corresponding thickness in a 1:500 scale simulation would be 3 ft

(0.91 m). Thick, turbulent boundary layers can be developed in two ways; (1) by providing sufficient length in the test section for natural development over a suitably rough surface; or (2) by installing devices at the test section entrance that will create an initial momentum deficit near the floor of the tunnel and that will accelerate the growth of the layer over a rough boundary. Both methods are of interest in developing techniques for modeling atmospheric boundary layers and, therefore, the method of natural development will dictate test-section length. Measurements of the development of rough-wall boundary layers having length scales of the order being considered here suggest a development length of approximately 60 ft (18.29 m) [9]. This is the distance from the test section entrance to the location of the model under test. Additional space will be required between the model and the end of the test section to allow for wake development and decay.

2.5 OTHER CONSIDERATIONS

It is conceivable that certain research activities will require the modeling of heat transfer phenomena or the effects of thermal stratification on boundary layer flows. Thermal modeling has not been addressed in the current design effort for two reasons. First, the general requirements for a thermal modeling capability within the Center for Building Technology have not been finalized. Second, construction costs for a boundary layer wind tunnel with state-of-the-art thermal modeling capabilities such as those described in reference 4 are estimated to be from three to four times the costs associated with a conventional facility. Nevertheless, the closed-circuit design described in this report is, in principle, adaptable to thermal modeling.

Consideration has also been given to the acoustic environment in the sense that provision has been made for the installation of silencers and the head loss due to these devices has been included in the estimates of the tunnel energy ratio. In addition to its adverse effect on the general working environment, noise produced by the drive section and return duct can cause very serious problems with the measurement of surface pressures on models under test. Because the fan requirements are only approximately established in this report, actual design of the silencers will be carried out after a specific fan has been selected. Finally, tunnel cooling may be an important factor, depending upon the tunnel configuration. If the closed-circuit arrangement with a thermal modeling capability is selected, tunnel cooling will be a part of the thermal capability. However, if a conventional closed-circuit arrangement is adopted, provision must be made to remove heat from the tunnel. Otherwise there will be serious problems with instrument drift and a very uncomfortable working environment in the test section. A feature of the closed-circuit design developed here is that space has been provided in the low-speed region of the tunnel for the installation of a heat exchanger. Cooling is not expected to be a serious problem with an open-circuit tunnel since normal air exchange in the space occupied by the tunnel will be sufficient to handle the heat generated under most operating conditions.

2.6 SPACE LIMITATIONS

The space proposed for housing the boundary layer wind tunnel facility is located in Building 202 on the NBS Gaithersburg site. At the present time this space is occupied by a number of small lab modules that were installed in what was originally a large open floor area. It is proposed that this open space be restored by removing a number of concrete masonry partition walls and a portion of the concrete floor slab installed at the second-floor level during the conversion to small lab modules.

The proposed renovation will provide a clear floor area of 29 x 132 ft (8.84 x 40.23 m) and a clear headroom of 21 ft (6.40 m). The roof structure consists of a metal deck placed over bar joists with a depth of 3 ft (0.91 m). This is of significance in the case of an open-circuit tunnel because of the additional area provided by the bar joists for the return flow. The floor consists of a 6 in (152 mm) concrete slab on grade. Removal of part of this slab will be required for a closed-circuit arrangement.

2.7 SUMMARY OF DESIGN CRITERIA

The design criteria developed up to this point can be summarized as follows:

Test section Dimensions:

Width = 10 ft (3.048 m).
Height = 6 ft (1.829 m).
Length = 60 ft (18.288 m) to turntable.

Speed Range:

Continuously variable from 1 to 80 fps (0.30 to 24.38 m/s).

Flow Quality:

Intensity of background turbulence ≈ 0.5 percent.
Maximum nonuniformity ≈ $\pm$ 1 percent.

Space Available for Construction:

Width = 29 ft (8.84 m)
Length = 132 ft (40.23 m)
Height = 21 ft (6.40 m)

3. CLOSED-CIRCUIT TUNNEL

3.1 GENERAL

The tunnel arrangement shown in figure 1 is believed to be a reasonable compromise among performance requirements on the one hand and constraints due to available

space, ease of fabrication and cost of construction on the other hand. The following sections of this report describe the design considerations that underlie the tunnel layout and the special features shown in figure 1.

3.2 TEST SECTION

The arrangement of the test section in figure 1 meets the general requirements for flow area and minimum working length prescribed by the performance criteria. A 12 ft (3.66 m) clearance is provided between the end of the tunnel and the laboratory wall line so that equipment can be moved to either side of the test section. Allowing room for the first and fourth corners, the wide-angle diffuser, the settling chamber and the contraction, 69 ft (21.031 m) are available for the test section. Sufficient space must be provided between the turntable and the first corner to allow room for wake development behind the models under test. This has been set at 14 ft (4.267 m) or approximately 20 model diameters, leaving 55 ft (16.764 m) between the test section entrance and the center of the turntable for boundary layer development. A second turnable is located near the test section entrance for conducting studies in smooth, uniform flow.

Nominal height of the test section is 6 ft (1.829 m), but this can be varied within the limits indicated by the dashed ceiling profile lines shown in figure 1. For the case of an empty tunnel the development of a turbulent boundary layer is given by the relationship

$$\delta = \frac{0.376\ X}{(R_e)^{1/5}} \tag{5}$$

where δ is the boundary layer thickness, X is the development length or distance downstream of the boundary layer origin and R_e is the Reynolds number based on the free-stream velocity and the development length [10]. The blockage effect of the boundary layer is given by the displacement thickness

$$\delta^* = \frac{\delta}{8} \tag{6}$$

It is seen that the depth of the boundary layer and the displacement thickness increase with decreasing tunnel air speed. For a speed of 10 fps (3.05 m/s), the boundary layer depth and displacement thickness at the turntable will be 1.03 and 0.13 ft (314 and 40 mm), respectively. Boundary layer development occurs on all four surfaces of the test section and, therefore, the net blockage is approximately (0.13) (perimeter) = 4.2 ft^2 (0.390 m^2). The corresponding ceiling adjustment required to maintain a zero longitudinal pressure gradient along the length of the test section will be 4.2/10 = 0.42 ft (128 mm).

The ceiling adjustment required for a rough-wall boundary layer can be estimated from the power law representation of the mean velocity profile for an urban exposure [11]

$$\frac{U_z}{U_\infty} = \left(\frac{z}{\delta}\right)^{0.33} \quad (7)$$

where U_z is the mean velocity at height z and U_∞ is the gradient or free-stream velocity. The corresponding displacement thickness is

$$\delta^* = 0.248\ \delta \quad (8)$$

Assuming a full-scale value of 1600 ft (488 m) for δ and a scale ratio of 1:400, the displacement thickness is (0.248)(1600)/400 = 1.0 ft (305 mm).

Blockage due to models immersed in a turbulent boundary layer is more difficult to assess, but the net effect will be an increase in the required ceiling adjustment. For this reason a maximum adjustment of 2 ft (610 mm) has been provided over the turntable. This range of adjustment also provides for a smooth transition from the 10 x 6 ft (3.048 x 1.829 m) test section to the 10 x 8 ft section (3.048 x 2.438 m) at the entrance to the first corner.

3.3 TURNING VANES

In order to limit losses to an acceptable level and maintain uniformity of flow, it is necessary to install turning vanes or cascades in the right-angle corners of closed-circuit tunnels. Experimental studies carried out by Salter [12] and by Winter [13] indicate that the most efficient turning vane arrangement consists of thin vanes fabricated from sheet metal and spaced so that the gap/chord ratio is approximately 0.25. As used here, "gap" refers to the vane spacing measured along the diagonal of a right-angle corner. Another commonly used measure of vane spacing is the pitch which is measured normal to the tunnel axis. Thus gap = $\sqrt{2}$ (pitch).

The vane profile recommended by Winter is shown in figure 2. The corresponding loss coefficient was found to be 0.033 at $R_e = 1.9 \times 10^6$. This does not include secondary flow losses at the vane roots (where the vanes intersect the tunnel walls) so a slightly higher loss coefficient, say 0.05, would be appropriate for design. It is expected that the performance of the turning vanes in the first corner will be adversely affected by the presence of a thick, turbulent boundary layer in the test section, or by the wake developed behind large bluff bodies tested in uniform flow. Because of this a higher loss coefficient, say 0.10, should be assumed for the first corner.

Specification of a gap/chord ratio does not, by itself, establish the chord length or gap dimension. Measurements of losses in rectangular ducts with short-radius bends [14] suggest that the aspect ratio (W/D where D is the radial dimension) should not be less than 3 under any circumstances and, preferably, should be greater than 6. Most of the closed-circuit tunnels described in reference 4 have cascades so proportioned that the aspect ratio of the slot between adjacent vanes ranges from 10 to 30. For the over/under closed-circuit arrangement shown of figure 1, the section width and height at the first corner

are 10 and 8 ft (3.048 and 2.438 m), respectively. Fifteen vanes with a pitch of 6 in (152 mm) would correspond to a vane gap of $6\sqrt{2} = 8.49$ in (215 mm). Thus the optimum chord length would be 4 x 8.49 = 33.94 in (862 mm) and the aspect ratio of the cascade slots would be 10 x 12/8.49 = 14.1. If the same vane gap is used in all four corners, the aspect ratio will reduce to 11.3 at the second corner and will increase to 17.0 at the third and fourth corners. These values are higher than is necessary to ensure good vane performance and, because of the lower speeds, it is likely that the gap/chord ratio for the third and fourth corners could be increased to about 0.5 without flow separation and stalling of the vanes. Selection of a smaller chord dimension would reduce the scale of disturbances produced by the turning vanes at the fourth corner and thus promote more rapid decay. However, the use of more than one chord and gap dimension would likely increase fabrication costs and would not lead to a significant improvement in quality of flow in the test section since a honeycomb and damping screens will accomplish the necessary flow conditioning. A typical vane cascade with optimum chord length is shown in figure 3.

Turning vanes of either variable or constant thickness are commercially available and it is doubtful that the fabrication of special vanes will prove to be economical. However, the discussion presented here can be used as a basis for turning vane evaluation and selection.

3.4 FIRST WIDE-ANGLE DIFFUSER

In a conventional closed-circuit tunnel, the drive section would be followed by a short round-to-square transition and a long plane-walled diffuser of square or rectangular cross section with a divergence angle (total included angle) of approximately 6 degrees. The length and aspect ratio of the diffuser would be so proportioned to make the tunnel cross section at the third corner comply with the pre-contraction tunnel section, in this case 16 x 12 ft (4.877 x 3.658 m). This would provide maximum flow area and would minimize losses through the third and fourth corners. Assuming an 8 ft (2.438 m) diameter for the drive section, the minimum diffuser length that can satisfy the limitation on divergence angle is approximately 76 ft (23.17 m). When combined with the length of the square-to-round transition, the required separation between the drive section and the entrance to the third corner is approximately 84 ft (26.60 m).

Although there is room to accommodate a 6-degree plane-walled diffuser, clearance at each end of the tunnel would be minimal and the cost of construction using either a lined pit or a cut-and-cover arrangement for the return circuit would be prohibitive. An attractive alternative is to use buried precast concrete pipe, a round-to-square transition and a wide-angle diffuser as indicated in figure 1. This will result in reduced operating efficiency, but the reduction in construction costs should be substantial.

The designation of "wide angle" as used here is somewhat arbitrary. Diffusers with divergence angles substantially greater than 8 degrees are often referred to as "wide angle" or "rapid expansion" diffusers. Although the divergence angle is only one of several parameters that determine diffuser performance,

there is general agreement that divergence angles should not exceed 7 or 8 degrees unless special measures are taken to guard against flow separation and stalling. The arrangement being considered here has a divergence angle of 22.6 degrees.

The diffuser expansion need not be limited to one plane and, in fact, it would be possible to make the transition from an 8 x 8 ft (2.438 x 2.438 m) section to a 16 x 12 ft (4.877 x 3.658 m) rectangular section using a wide-angle diffuser with a two-plane expansion. The problem with this approach is that the width and depth of the excavation could introduce additional construction problems such as foundation underpinning. In addition, the length required upstream of the settling chamber for the fourth corner would be approximately the same as the arrangement shown in figure 1 for which a second wide-angle diffuser is required to make the transition from the fourth corner to the settling chamber. The arrangement shown in figure 4 is a plane-walled diffuser with single-plane expansion. The area ratio (outlet/inlet) is 1.50 and the ratio of length to inlet width is 1.25. According to the diffuser performance data presented in reference 15, this diffuser will exhibit transitory three-dimensional flow separation and will operate just outside of the steady two-dimensional separated flow regime. Clearly, this arrangement would result in low diffuser efficiency and poor tunnel performance, the most serious effect being unsteadiness or surging in the tunnel speed.

Instabilities in wide-angle diffusers are usually associated with flow separation at some point along the diffuser wall where the momentum in the boundary layer is insufficient to overcome the boundary shear and the adverse pressure gradient. Techniques that have been used to cure transitory flow separation and stall in diffusers include removal of the boundary layer through suction slots and the addition of momentum to the boundary layer with devices such as vortex generators. The best solution is to avoid problems with separation and stall through proper choice of diffuser geometry.

Schubauer and Spangenberg [16] demonstrated the effectiveness of diffusing screens in preventing boundary layer separation and in restoring separated flows in diffusers with very large angles of divergence. Moore and Kline [17] showed that good performance can be obtained from two-dimensional wide-angle diffusers by using flat-plate splitter vanes installed close to the diffuser throat. This technique was refined by Cochran and Kline [18] and a three-dimensional version has been used successfully in at least one large boundary layer wind tunnel of recent construction [4]. Whether one chooses diffusing screens or vanes, the resulting losses in the diffuser will be greater than would occur in a conventional diffuser without flow separation. This is the price to be paid for improved diffuser performance.

An additional benefit of diffusing screens is the reduction of turbulence since they also act as damping screens. Because of this, diffusing screens are usually installed ahead of the settling chamber in blowdown tunnels (i.e., open-circuit tunnels with the drive section located ahead of the test section). Their main disadvantage is that, for a given diffuser, the losses are usually higher than those produced by vanes. Vanes are usually cheaper and easier to install, but their greatest advantage in the application being considered here

is that they can also serve as acoustic silencers. An alternative would be to install annular silencers at the fan outlet with resulting losses considerably higher than those produced by a wide-angle diffuser fitted with vanes.

Based upon the findings presented in references 17 and 18, it is possible to establish a three-dimensional vane arrangement (see figure 4) that can be expected to perform adequately. However, since definitive design criteria are not available, performance should be confirmed using a scale model of the diffuser that includes the circular duct upstream of the diffuser and the turning vanes in the third corner directly downstream of the diffuser. Also, the prototype should be designed to allow for fine adjustment of the diffuser vanes because of uncertainties with respect to scale effects.

For purposes of design it is necessary to estimate the energy loss through the diffuser and this requires some knowledge of its performance characteristics. Various parameters have been used to describe diffuser performance, one of the more common parameters being the nondimensional static-pressure recovery coefficient

$$C_{pr} = \frac{P_2 - P_1}{1/2\ \rho U_1^2} \tag{9}$$

where the subscripts 1 and 2 refer to the diffuser inlet and outlet sections, respectively. Neglecting for the moment such problems as nonuniform distribution of velocity and pressure, and assuming no energy losses, the theoretical maximum value of the static-pressure recovery coefficient for a diffuser with inlet area A_1, and outlet area A_2 is

$$\hat{C}_{pr} = 1 - \left(\frac{A_1}{A_2}\right)^2 \tag{10}$$

Thus, for the wide-angle diffuser arrangement shown in figure 4, the upper limit on the static-pressure recovery coefficient would be $1 - (64/96)^2 = 0.56$.

Equation 9 is valid only if the flow is incompressible, the flow at the diffuser inlet is uniform and axial, and the distribution of the static pressure across the diffuser outlet is uniform. While the flow being considered here can be treated as incompressible, the swirl component imparted by the fan to the approach flow and the boundary layer development along the circular duct and circular-to-square transition will contribute to a nonuniform velocity distribution at the diffuser inlet. To account for this nonuniformity, a kinetic energy coefficient, α, and a potential energy coefficient, β, are introduced

where

$$\alpha = \frac{1}{AU_A} \int_A (1/2\ \rho U^2) U dA / (1/2\ \rho U_A^2)$$

$$= \frac{1}{AU_A^3} \int_A U^3 dA \tag{11}$$

and

$$\beta = \frac{1}{AU_A} \int_A P U dA / P_A$$

$$= \frac{1}{AU_A P_A} \int_A P U dA \tag{12}$$

The loss in total pressure, P_t, over the length of the diffuser can be expressed as

$$P_{t1} - P_{t2} = \alpha_1 (1/2\ \rho U_{A1}^2) - \alpha_2 (1/2\ \rho U_{A2}^2) - (\beta_2 P_{A2} - \beta_1 P_{A1}) \tag{13}$$

where the subscript A denotes an area-averaged quantity. The loss in total pressure is usually expressed in the form of a total-pressure loss coefficient

$$K_t = \frac{P_{t1} - P_{t2}}{\alpha_1 (1/2\ \rho U_{A1}^2)} \tag{14}$$

Reference 15 presents contours of static-pressure recovery coefficients and tentative values of total-pressure loss coefficients for diffuser geometries similar to that shown in figure 4. Suggested values for C_{pr} and K_t are approximately 0.40 and 0.18, respectively.

Although reference 18 does not consider diffuser length ratios (length/inlet width) of less than 4 and in most cases works with length ratios of 8, the data for divergence angles of from 20 to 30 degrees indicate that a properly designed diffuser with vanes should operate at about 80 percent of the theoretical upper limit on C_{pr}. This compares with an average value of about 55 percent for a wide-angle diffuser without vanes. With regard to the total-pressure loss coefficient, reference 18 indicates K_t = 0.15 to 0.20 for a vaned diffuser over the same range of divergence angle. For diffusers without vanes, K_t = 0.25 to 0.55. When compared with the values of C_{pr} and K_t suggested in reference 15, the addition of vanes to the diffuser shown in figure 4 would be expected to improve C_{pr} slightly (0.8 x 0.56 = 0.45 vs 0.40) and K_t would be expected to remain about the same (0.15 to 0.20 vs 0.18). Thus the major advantages of a vaned diffuser in this case are the prevention of transitory three-dimensional flow separation and the use of the vanes as acoustic silencers. In estimating pressure profiles and power requirements, values of C_{pr} = 0.40 and K_t = 0.18 have been assumed.

3.5 SECOND WIDE-ANGLE DIFFUSER

The floor profile for diffuser No. 2 connecting the fourth corner with the settling chamber is shown in figure 5. The approach taken here is to eliminate the potential for flow separation by adding diffusing screens as described in reference 16. While a vaned diffuser would be more efficient, vanes would generate wakes directly ahead of the settling chamber and this would require damping screens with higher combined loss coefficients to produce the same quality of flow at the entrance to the test section.

The principle underlying the selection and placement of diffusing screens in a wide-angle diffuser is to forestall flow separation by reducing the adverse pressure gradient over the length of the diffuser. In effect, the diffuser and screens are proportioned so as to make the static-pressure recovery coefficient equal to zero. This can be accomplished by using a single diffusing screen with a high loss coefficient, or by using multiple diffusing screens with lower loss coefficients. However, the spacing of the screens along the length of the diffuser must be close enough to prevent flow separation from occurring along the diffuser walls between the screens.

In reference 16 the diffuser efficiency is defined as the ratio of gain in potential energy to loss in kinetic energy. Thus the efficiency, E', between any two sections 1 and 2 of the diffuser is

$$E'_{1,2} = \frac{\beta_2 P_{A2} - \beta_1 P_{A1}}{\alpha_1 (1/2\ \rho U_{A1}^2) - \alpha_2 (1/2\ \rho U_{A2}^2)} \tag{15}$$

If diffusing screens with loss coefficients K_1 and K_2 are installed at sections 1 and 2, respectively, and if their effect is to make P and U uniform over each section, the diffuser efficiency from the downstream side of screen 1 to the downstream side of screen 2 will be

$$E_{1,2} = E'_{1,2} - \frac{K_2}{\left(\frac{A_2}{A_1}\right)^2 - 1} \tag{16}$$

The wide-angle diffuser shown in figure 5 has an area ratio of 2 and horizontal and vertical divergence angles of 36.9 degrees. There is very little information in the literature regarding the performance of plane-walled diffusers with a two-plane expansion and it is necessary to infer certain characteristics from diffusers with single-plane expansions. Using equations (9) and (10) and assuming that the diffusing screens will be fully effective in promoting uniform flow throughout the diffuser, the efficiency, exclusive of screen losses, can be expressed as

$$E' = \frac{C_{pr}}{\hat{C}_{pr}} \tag{17}$$

Therefore, it will suffice to estimate C_{pr}. If it is further assumed that the static-pressure recovery coefficients suggested by reference 18 are typical of wide-angle diffusers operating without separation, then $C_{pr} \simeq 0.8\ \hat{C}_{pr}$ and $E' \simeq 0.8$. Setting E = 0 in equation (16), the required screen loss coefficient for a given screen spacing is

$$K_1 = 0.8 \left[\left(\frac{A_1}{A_0} \right)^2 - 1 \right] \tag{18}$$

To reduce the likelihood of flow separation at the juncture of the fourth-corner outlet section and the wide-angle diffuser section, a smooth transition is provided by the circular arc with 6 ft (1.829 m) radius as shown in figure 5. To simplify fabrication the transition is made an integral part of the fourth-corner assembly and the plane of connection with the diffuser is a convenient location for the first diffusing screen. From equation (18) the required loss coefficient is K = 0.23. If the second diffusing screen is placed at the end of the diffuser, a loss coefficient of K = 1.70 will be required.

Although this arrangement will satisfy the requirement that E = 0, it does not guarantee the absence of flow separation along the diffuser walls. The most likely location for separation to occur is along the corners of the diffuser downstream of the first screen. If an additional screen is installed 2.5 ft (762 mm) upstream of the diffuser outlet, the respective loss coefficients for the first, second and third diffusing screens will be 0.23, 0.68 and 0.56. As a part of this design effort, preliminary studies carried out on a diffuser of similar geometry indicate that three screens are sufficient to suppress flow separation. Screens having identical K factors may be used so long as K is not less than 0.68. A logical choice for uniform screen type would be 20 mesh (20 wires/in) and wire diameter of 0.010 in. (0.25 mm) which is readily available in widths of 12 ft (3.66 m) or more and for which K ≃ 0.70.

It is of interest that Schubauer and Spangenberg [16] explored the possibility of using curved diffuser walls of optimum profile while carrying out their studies of diffusing screens in conical diffusers. Theoretical and experimental studies of optimum wall profiles for axisymmetric diffusers are reported in reference 19. With optimum wall profile and careful design and location of a single diffusing screen with nonuniform loss coefficient, it is possible to achieve moderate levels of pressure recovery and highly uniform flow at the outlet of axisymmetric diffusers having very small length/diameter ratios. Although it is less efficient, the plane-walled diffuser shown in figure 5 is relatively simple to fabricate.

3.6 SETTLING CHAMBER

The settling chamber provides space for flow modification or conditioning devices located directly upstream of the wind tunnel contraction. Since the contraction also functions as a flow modification device and influences the

flow for some distance upstream, the design of the settling chamber and the design of the contraction are interrelated.

3.6.1 Damping Screens

The most common pre-contraction flow conditioning device is the damping screen. Its function is to accelerate the decay of incident turbulence and promote uniformity of the flow. On the basis of extensive tests concerned with the modification of turbulence intensity by wire mesh screens, Dryden and Schubauer [20] suggested that the mean intensity of turbulence in a flow passing through a screen is reduced by the ratio

$$\frac{I_2}{I_1} = \frac{1}{\sqrt{1 + K}} \tag{19}$$

where I_1 is the turbulence intensity upstream of the screen, I_2 is the downstream intensity, and K = the head-loss or pressure-drop coefficient. The value of K is dependent upon Reynolds number, but may be assumed to be constant for screens with solidity ratios (solid area/total area) of less than about 0.6 and with $R_e > 150$. For $R_e < 75$, K increases rapidly with decreasing speed.

In view of the form of equation (19), obviously it is more efficient to use n screens with head-loss coefficient K than it is to use one screen with head-loss coefficient nK to achieve the desired reduction in turbulence intensity. While there is a minimum spacing of screens required to produce maximum damping of turbulent fluctuations (400 to 500 wire diameters), screen spacing is usually dictated by the working space required for cleaning the screens. Thus the screen spacing should not be less than about 2 ft (610 mm).

With regard to nonuniformity of flow, it can be shown [21] that if $\tilde{U}_1 = U_A + u_1$ is the local longitudinal velocity far upstream and $\tilde{U}_2 = U_A + u_2$ is the corresponding value far downstream of the screen, where the subscript A denotes averaging over the tunnel cross section, then

$$\frac{u_2}{u_1} = \frac{2 - K}{2 + K} \tag{20}$$

so that nonuniformity of flow is completely removed by a screen with K = 2. More recent work and measurements carried out in actual wind tunnel installations suggest that the optimum head-loss coefficient for the reduction of spatial variations in velocity is approximately 2.8 [5,22].

3.6.2 Honeycomb

Although wire mesh screens can be very effective in damping turbulent fluctuations and in reducing non-uniformity of flow, they are not particularly

effective in removing steady transverse components of velocity induced by the fan in closed-circuit tunnels or by the inlet in open-circuit tunnels. To remove these unwanted components, it is usual practice to place a honeycomb directly upstream of the damping screens. For tunnels of the size being considered here, satisfactory performance has been obtained with a cell diameter of 2 inches (50.8 mm) or less and a cell length of about 8 times the cell diameter [22].

When a honeycomb is used as a flow conditioner, it is necessary to provide sufficient length in the downstream portion of the settling chamber to allow the turbulence generated by the honeycomb to decay before the flow enters the contraction. Alternatively, one or more damping screens can be placed downstream of the honeycomb. Prior to the work of Loehrke and Nagib [23], the mechanisms by which honeycombs suppress incoming turbulence and generate turbulence in the exiting flow were not well understood. As a result, the benefits expected of honeycomb installations were not always realized and in certain cases the flow quality was actually reduced by the installation of a honeycomb [24].

The work reported in reference 23 indicates that the suppression of turbulence in the flow entering a honeycomb is due in large part to the inhibition of the lateral components of fluctuating velocity. Flow visualization studies show that most of the suppression occurs within the first 5 to 10 diameters along the honeycomb cells and that the predominant mechanism by which turbulence is generated in the flow exiting the honeycomb is shear-layer instability. By placing a fine-mesh damping screen (K = 0.86) within 5 cell diameters of the downstream face of the honeycomb, Loehrke and Nagib showed that the shear layers in the exiting flow can be modified, leading to very rapid decay of turbulence and reducing the intensity to approximately 2 percent at a downstream distance of from 30 to 40 cell diameters.

3.6.3 Arrangement of Flow Conditioners

The recommended arrangement of the settling chamber is shown in figure 6. A 2 ft (610 mm) space is provided at the settling chamber inlet to gain access to the honeycomb and to allow for cleaning of the back side of the last diffusing screen in the wide-angle diffuser. This space also allows for some lateral adjustment of the flow before entering the honeycomb. Because they are inexpensive and readily available, 2 in (50.8 mm) O.D. cardboard tubes with a length of 10 diameters or 20 in (508 mm) are recommended for construction of the honeycomb.

Following the recommendation of reference 23, a damping screen is installed approximately 4 tube diameters or 8 in (203 mm) from the downstream face of the honeycomb. The choice of K value for the damping screen does not appear to be critical. However, a screen with K = 0.86 was used in the studies reported in reference 23 and this is close to the head-loss coefficient K = 0.70 selected for the diffusing screens. With this combination of honeycomb and damping screen, the intensity of the streamwise component of turbulence should be approximately 2 percent at 5 to 6 ft (1.52 to 1.83 m) downstream of the screen.

Additional reduction of turbulence will be achieved in the contraction and this is discussed later.

The loss coefficients for the honeycomb and damping screen are shown in reference 23 to be directly additive. Reference 24 suggests K = 0.30 for tubular honeycomb of the type used here. This value corresponds to a length/diameter ratio of 6 and, therefore, K = 0.5 would be a reasonable choice for a length/diameter ratio of 10. Thus the combined loss coefficient for the honeycomb and damping screen would be K = 0.5 + 0.7 = 1.2.

In order to assess the effectiveness of the honeycomb/screen combination in the settling chamber, the level of turbulence directly ahead of the honeycomb must be known. Based on information presented in reference 25, a turbulence intensity of about 12 percent toward the end of a well-designed return circuit is considered reasonable. For the tunnel being considered here, the use of a relatively rough circular duct and a wide-angle diffuser in the return circuit can be expected to result in a higher level of turbulence at the fourth corner, say 20 percent. With a loss coefficient of K = 0.70 for each of the three diffusing screens, the reduction in the r.m.s. level of the streamwise fluctuations as the flow passes through the second wide-angle diffuser will be about 55 percent, according to equation (19). Accounting for the change in mean velocity between the fourth corner and the settling chamber, the intensity of the streamwise component of turbulence just upstream of the honeycomb will be about 18 percent, based on the local flow velocity. This estimate does not account for natural decay or production of turbulence by the second wide-angle diffuser. Nevertheless, the honeycomb/screen combination appears to be far more efficient than are multiple damping screens or a honeycomb and screens without proper attention given to the honeycomb-screen spacing. Assuming that a series of damping screens with K = 0.70 were substituted for the honeycomb/screen combination, 8 screens would be required to achieve the same reduction in turbulence intensity. The combined head-loss coefficient would be 8 x 0.70 = 5.6 vs. 1.2 for the honeycomb/screen combination.

3.7 EFFECT OF THE CONTRACTION

The contraction section for the tunnel arrangement shown in figure 1 has a contraction ratio (inlet area/outlet area) of 3.2:1 and an aspect ratio (width of section/height of section) of 1.33:1 at the inlet and 1.67 at the outlet. Although the details of the contraction design are addressed later, the effects of the contraction on the flow are almost entirely dependent upon the contraction ratio. Therefore, these effects are addressed here in the context of flow conditioning.

3.7.1 Nonuniformity of the Mean Flow

An important function of a wind tunnel contraction is the generation of uniform mean flow at the entrance to the test section. Assuming that the flow in the contraction is incompressible, inviscid and steady, it can be shown [26] that the improvement in flow uniformity on passing through the contraction is given by

$$\frac{(U_{A2} - \tilde{U}_2)/U_{A2}}{(U_{A1} - \tilde{U}_1)/U_{A1}} = \frac{\tilde{U}_1 + U_{A1}}{\tilde{U}_2 + U_{A2}} \cdot \frac{U_{A1}}{U_{A2}} \simeq \frac{1}{C_R^2} \tag{21}$$

In this expression U_A is the area-averaged mean velocity, $\tilde{U}$ is the local mean velocity, C_R is the contraction ratio and the subscripts 1 and 2 denote the inlet and outlet sections, respectively.

For a contraction ratio of 3.2:1 the attenuation factor for nonuniformity of mean velocity is 0.10. Thus the local nonuniformity downstream of the honeycomb/damping screen should not deviate from the mean velocity by more than 10 percent if the target uniformity of $\pm$ 1 percent in the test section is to be met. Of course this excludes the boundary layer region at the walls of the contraction. With reasonable care in the installation of the diffusing screens, honeycomb and damping screen, there should be no difficulty in satisfying the 10 percent limitation on velocity deviation directly upstream of the contraction.

3.7.2 Reduction of Turbulence

The effects of a contraction on free-stream turbulence using the simple concept of preferential stretching and shortening of cylindrical vortex filaments and using the concept of rapid distortion (sometimes referred to as the linear theory) are summarized in reference 26. Applying the concept of preferential stretching and shortening, the intensities of the three components of turbulence, u, v and w, are attenuated by an axisymmetric contraction with C_R = 3.2:1 as follows:

$$\frac{I_{u2}}{I_{u1}} = \frac{1}{C_R^2} = 0.10 \tag{22}$$

$$\frac{I_{v2}}{I_{v1}} = \frac{I_{w2}}{I_{w1}} = \frac{1}{\sqrt{C_R}} = 0.56 \tag{23}$$

Rapid distortion theory leads to the following relationship between pre- and post-contraction turbulence intensities with C_R = 3.2.

$$\frac{I_{u2}}{I_{u1}} = 0.17 \tag{24}$$

$$\frac{I_{v2}}{I_{v1}} = \frac{I_{w2}}{I_{w1}} = 0.49 \tag{25}$$

Experimental studies carried out by Ramjee and Hussain [27] using axisymmetric contractions with contraction ratios ranging from 11:1 to 100:1 indicate that the rapid distortion theory overestimates the attenuation of the intensity of the streamwise component and underestimates that of the transverse components. For contraction ratios of 11:1 or less, data presented in reference 27 suggest that $I_{v2}/I_{u2} \simeq 1.3$. Therefore, use of equation (25) will provide a conservative estimate of the turbulence intensity at the test section entrance. Assuming that the honeycomb/screen combination installed in the settling chamber will perform as expected ($I_{u1} = I_{v1} = 0.02$), the turbulence intensity at the entrance to the test section should be approximately 1 percent ($I_{v2} = 0.49\ I_{v1}$). Further reduction of the turbulence intensity will require additional damping screens in the settling chamber.

3.8 DESIGN OF THE CONTRACTION

Factors that influence the choice of contraction geometry include the degree to which spatial irregularities in the velocity distribution are to be reduced, the intensity of turbulence expected at the entrance to the test section, and the effect of the contraction ratio on tunnel power consumption. If highly uniform flow of very low turbulence ($\sqrt{\overline{u^2}}/U < 0.001$) is desired, contraction ratios of 9 or greater are usually required. In the case of closed-circuit tunnels the use of large contraction ratios results in relatively low speeds in the return section and a corresponding reduction in losses, particularly at the third and fourth corners and at the damping screens. For an open-circuit tunnel the greatest reduction in losses occurs at the damping screens and, to a lesser extent, at the tunnel inlet. Factors that argue against a large contraction ratio are the increased floor area and headroom required for the third and fourth corners and for the settling chamber, the increased length of the contraction (which is usually at the expense of useable test section length), and the cost of construction.

Available floor space in this case limits a closed-circuit design to an over/under arrangement as shown in figure 1. The dimensions of the contraction inlet could be increased beyond the 16 x 12 ft (4.877 x 3.658 m) section indicated, but this would have to be at the expense of clear working space along the sides of the settling chamber (already considered to be the minimum acceptable) and headroom available for installation or replacement of the diffusing and damping screens. Since the arrangement of the return duct, the third and fourth corners, and the wide-angle diffusers is dictated by factors other than the contraction ratio, a contraction ratio larger than the value of 3.2 used here would not lead to a significant reduction in power requirements. If a lower level of turbulence at the entrance to the test section is desired, this can better be achieved with the installation of additional damping screens in the settling chamber.

For the reasons just described, the contraction ratio is by far the most important parameter in the design of a wind tunnel contraction. Once this ratio has been selected, the wall profiles and the overall length of the contraction must be established. Ideally, the contraction should operate over the design speed

range without flow separation, the boundary layer should be relatively thin, and the exit velocity should be highly uniform. These features should be achieved within the shortest possible length.

As Bradshaw and Pankhurst [25] have noted, there is no method, either in two or three dimensions, that can be considered entirely satisfactory for contraction design. Although various analytical techniques have been used in the design of axisymmetric and two-dimensional contractions, many low-speed tunnels of recent construction use contractions that either are adaptations of previous "good" designs that have given satisfactory performance, or are based upon systematic studies using scale models. A major problem in contraction design is that for any contraction of finite length, the flow along the wall must pass through points of minimum and maximum velocity. Thus there is a region near each end of the contraction where the pressure gradient along the wall is adverse and where, under certain conditions, separation of the boundary layer can occur. Flow separation is a distinct possibility in the case of small contraction ratios where the flow accelerations may be too small to overcome locally adverse pressure gradients, and in the case of two- and three-dimensional contractions where secondary flows develop in the boundary layer at the corners.

The contraction profile considered here is an adaptation of one described in reference 28. Tests carried out in both model and full scale indicate a highly uniform exit velocity and the absence of boundary layer separation. The wall profile, derived from a 4th order polynomial, has the form

$$Y = -3h\left(1-\frac{X}{L}\right)^4 + 4h\left(1-\frac{X}{L}\right)^3 \qquad (26)$$

where X, Y, h and L are as defined in figure 7.

Based on overall dimensions of contractions that have demonstrated good performance and have contraction ratios close to the ratio being considered here [4], a contraction length of 14 ft (4.267 m) was selected. To simplify fabrication of the contraction and to make it easier to install corner fillets if their use is desired at some future time, the same profile is used for all four walls. Dimensionless coordinates of the wall profile, the cross sectional area, the local pressure coefficient based on average axial velocity and referenced to the static pressure at the outlet, and the pressure gradient along the axis of the contraction are listed in table 1. The local pressure coefficient and the pressure gradient are plotted in figure 8. Also plotted in figure 8 are C_p and its gradient for two wind tunnel contractions of recent construction [29,30] whose dimensions are reasonably close to those of the contraction being considered here. Note that the pressure gradients for these two tunnels are approximate, having been estimated from the distribution of C_p since the exact form of the wall profiles is not known. Overall dimensions of the three contractions are listed in table 2. It can be seen from figure 8 that the pressure gradient in the "core flow" is favorable for all three contractions, the maximum absolute value for the proposed contraction being approximately 90 percent of the other two.

While such a comparison may be reasonably accurate for the flow in the core of the contraction, it is not possible to extend this comparison to the flow along the walls or, more importantly, to the flow in the corner regions where boundary layer separation will occur first.

To assess the potential for boundary layer separation, reference is made to the work of Morel on axisymmetric contractions [31] and on two-dimensional wind tunnel contractions [32]. The approach taken by Morel was to solve the Euler equations of motion using a finite-difference procedure. The boundary layer displacement thickness was assumed to be much smaller than the transverse dimensions of the contraction so that the flow could be treated as potential flow. The boundary conditions were the wall profiles consisting of two smoothly matched arcs with apex at the ends of the contraction and a finite length of straight duct at each end of the contraction where the velocity profile approaches uniform flow. Using the results of this analysis, Morel established a procedure for selecting a shape parameter and contraction length that just avoids boundary layer separation and minimizes the boundary layer thickness. Based on the analysis of more then 100 configurations with power-law wall shapes of order ranging from 2 to 5, Morel concluded that two smoothly joined cubic arcs satisfy the separation criterion for an axisymmetric contraction with relatively short length. The analysis of two-dimensional contractions reported in reference 32 was limited to wall profiles consisting of two cubic arcs.

The three-dimensional contraction used in the tunnel arrangement shown in figure 1 can be considered to be bounded by the two-dimensional and axisymmetric cases analyzed by Morel. If the contraction is assumed to be two-dimensional, the contraction ratio is equal to the ratio of the inlet height to outlet height, or 2.0. The inflection point of the wall profile, which is located at a distance of L/3 from the inlet plane, can be taken as the equivalent of the match point for Morel's cubic arcs. An additional parameter required to establish Morel's separation criterion is the distance from the virtual origin of the boundary layer to the inlet plane of the contraction which is taken to be the distance to the last damping screen in the settling chamber; approximately 4 ft (1.22 m) in this case. The wall pressure coefficient associated with separation is $C_{pi} = 0.41$ and the expected value is $C_{pi} = 0.31$ where

$$C_{pi} \equiv 1 - (U_i/V)^2 \tag{27}$$

In this definition of C_{pi}, U_i is the mean velocity sufficiently far upstream of the inlet for the flow to be considered uniform and V is the local velocity just outside of the boundary layer.

For the axisymmetric case the contraction diameters are taken to be 4 times the hydraulic radius at the inlet and outlet planes of the three-dimensional contraction. The corresponding contraction ratio is 3.34 and the critical value of C_{pi} is again 0.41. This compares with an expected value of $C_{pi} = 0.28$.

Since these pressure coefficients are based on wall profiles consisting of cubic arcs, they are not directly applicable to the 4th order profile being considered here. For an axisymmetric contraction with contraction ratio of 9, Morel investigated the effect of different power-law wall shapes on C_{pi} and on the

pressure gradient term used to establish the criterion for flow separation. The value of C_{pi} for a 4th order power law curve is approximately 1.35 times that for a cubic arc while the pressure gradient term is essentially unchanged. The effect for a contraction ratio of about 3 probably would be less. Nevertheless, the effects of secondary flow in the boundary layer adjacent to the corners of the three-dimensional contraction are cause for concern and the final design should allow for the possible installation of corner fillets to reduce the tendency for secondary flows to develop in the corners of the contraction.

With regard to the potential for boundary layer separation near the end of the contraction, Morel's results for an axisymmetric contraction indicate the local pressure coefficient at the wall is not strongly dependent on the choice of power-law wall profile [31]. Since the length selected for the contraction being considered in this design is slightly longer than the "optimum" length for a wall profile consisting of matched cubic arcs, separation near the end of the contraction is not likely to be a controlling factor.

3.9 ESTIMATION OF ENERGY RATIO

The energy ratio for a wind tunnel is defined as the ratio of the flux of kinetic energy at the test section entrance to the rate of work done by the drive section on the fluid. Assuming uniform flow at the test section entrance, the energy ratio can be expressed as

$$E.R. = \frac{1/2\ \rho U_o^3 A_o}{A_o U_o\ \Delta P_t} \tag{28}$$

where A_o and U_o are the area and velocity, respectively, at the test section entrance and ΔP_t is the total head loss along the path length of the tunnel.

The total head loss, ΔP_t, is equal to the sum of the losses due to the individual tunnel components and may be expressed as

$$\Delta P_i = K_i\ 1/2\ \rho U_i^2 = K_{oi}\ 1/2\ \rho U_o^2 \tag{29}$$

and thus

$$K_{oi} = K_i \left(\frac{U_i}{U_o}\right)^2$$

$$= K_i \left(\frac{A_o}{A_i}\right)^2 \tag{30}$$

where U_i is the appropriate reference velocity for calculating the head loss through the tunnel component. For a tunnel with n discrete components that contribute to the total head loss, we have

$$\Delta P_t = \sum_{i=1}^{n} K_{oi} 1/2 \, \rho U_o^2 \tag{31}$$

and

$$E.R. = \frac{1}{\sum_{i=1}^{n} K_{oi}} \tag{32}$$

In most cases K_i is related to the local Reynolds number with K_i increasing with decreasing R_e. For purposes of estimating power requirements the losses are based on the K_i associated with maximum R_e where it is usual to observe only a weak dependence of K_i on R_e.

Table 3 lists the tunnel components, the estimated values of K_i, the source of these estimates and the corresponding values of K_{oi}. For purposes of establishing the maximum power requirements, the test section is assumed to contain a bluff body (circular cylinder) spanning the test section from floor to ceiling and having a characteristic dimension of 0.5 ft (152 mm). Also listed in table 3 is the percentage contribution of each component to the total head loss. The estimated energy ratio for the closed-circuit tunnel is 0.53.

The energy ratio is an indicator of tunnel efficiency and a well-designed tunnel is characterized by both a high energy ratio and satisfactory performance characteristics. Aeronautical tunnels with a long diffuser in the return circuit and operating without screens or other flow conditioning devices may have energy ratios of 5 or greater [24].

3.10 PRESSURE PROFILES

Once the head losses have been estimated, it is possible to calculate the profiles of total pressure and static pressure around the tunnel circuit. The total pressure profile reflects the head losses along the tunnel circuit while the static pressure profile is used to obtain the design loads for the various tunnel components. The last two columns of table 3 list the total pressure and static pressure, respectively, for an operating speed of 80 fps (24.38 m/s). The corresponding profiles are plotted in figure 9.

Unless provisions are made for venting a closed-circuit tunnel, the static pressure will adjust to the leakage that is almost always present in construction joints, screen slots, etc. For a "sealed" tunnel, the static pressure in regions of high velocity will be lower than the outside ambient pressure. This usually means that the test section will operate at a static pressure substantially below the outside ambient pressure with the result that any

leaks in the test section will act as inward-directed jets that can disrupt the growth of boundary layers and alter the base pressure for models undergoing tests. This problem can be reduced by exercising great care in the design and construction of the test section, but the most effective step is to intentionally vent the test section to the outside ambient pressure. This is usually done at the downstream end of the test section so that most of the test section operates just slightly above ambient pressure. Sealing of fixtures such as turntables, cable entries, etc. then becomes relatively unimportant. The penalty for venting the test section is an increase in static pressure throughout the tunnel and this can lead to significant increases in design loads for components in regions of very low speed, e.g. the third and fourth corners and the settling chamber. The static pressure profile plotted in figure 9 assumes venting just downstream of the first corner.

3.11 FAN SELECTION

Knowing the energy ratio of the tunnel, the relationship between the flow rate and the head loss can be obtained. This relationship is plotted as the tunnel load characteristic in figure 10. Note that the tunnel load characteristic at very low flow rates is underestimated because of the dependence of loss coefficients on the Reynolds number. This will influence the required fan speed at low rates of flow but will not affect the fan size requirements.

Characteristic curves for a typical axial flow fan with an 8 ft (2.438 m) diameter casing are also plotted on figure 10. The operating point corresponding to maximum fan efficiency (approximately 76 percent for this fan) is indicated on each of the fan characteristic curves.

To ensure stable tunnel speed, the fan characteristic curves should have relatively steep slopes over the operating range and should intersect the tunnel load characteristic curve at angles approaching 90 degrees. From figure 10 it is seen that stability may present a problem for tunnel speeds of less than about 30 fps (9.14 m/s). Methods that have been used to overcome this problem include; (1) equipping the tunnel with a bypass section so that the flow rate through the fan remains high for all tunnel speeds, (2) using a fan with continuously variable, remote-controlled pitch setting or (3) using a fan with incremental pitch settings (made with the fan stopped). The first two methods, while more convenient, are relatively expensive. The third method offers substantial improvement in performance at little additional cost. The dashed line in figure 10 is a fan characteristic for the case of selectable-pitch blades set at a relatively flat angle of attack.

For a maximum tunnel speed of 80 fps (24.38 m/s), the corresponding flow rate is 288,000 cfm (136 m^3/s) and the tunnel load characteristic indicates a head loss of approximately 2.65 in (67.3 mm) of water. The required fan speed for a typical 8 ft (2.438 m) diameter axial flow fan is about 690 RPM and the corresponding speed of the blade tips is 289 fps (88.09 m/s). This is in general agreement with the maximum tip speeds for the low-speed tunnels described in reference 4 and easily satisfies the recommendation of reference 25 that tip speed not be allowed to exceed half the speed of sound. Based on the tunnel load characteristic and a maximum operating speed of 80 fps (24.38 m/s), an

axial flow fan with an 8 ft (2.438 m) casing diameter will be adequate. To ensure stable operation at low tunnel speeds, $U_o < 30$ fps (9.14 m/s), the fan should be equipped with selectable-pitch blades.

3.12 POWER REQUIREMENTS

The power required at the fan shaft is plotted in figure 11. This curve is based on an overall fan efficiency of about 72 percent and does not account for uncertainties in the tunnel energy ratio, motor efficiency or mechanical losses between the motor and fan. Therefore, motor selection should be based on a power requirement approximately 10 percent greater than is indicated by figure 11 or about 180 hp (134 kW). A motor of this size can be housed within the fan nacelle with direct coupling to the fan hub.

For motors larger than 150 hp (112 kW), the size selection offered by most manufacturers is limited to increments of 50 hp (37 kW). Allowing for a 10 percent margin on required power, a 150 hp (112 kW) drive motor will be adequate for tunnel speeds of up to 75 fps (22.86 m/s). The consequences of setting the maximum operating speed below the target value of 80 fps (24.38 m/s) are discussed later in the context of an open-circuit tunnel.

3.13 MOTOR AND CONTROLLER

The size of motor being considered here and the fact that it will be coupled directly with the fan preclude the use of a number of mechanical and electro/mechanical devices that are available for speed control. Of the five means of electrical speed control described in reference 38, it appears that frequency regulation of an induction motor or voltage regulation of a direct current motor are the only practical alternatives.

The principal advantages of frequency regulation are the high reliability and low maintenance inherent in an induction motor and the fact that the torque/speed characteristic changes only slightly as the supply frequency changes. The disadvantages of this method of speed regulation are the relatively high cost of the controller and the limited range of speed regulation. The "turn-down ratio" or factor by which the speed can be changed is limited to about 10:1 so that the minimum tunnel speed will be approximately 10 percent of the maximum speed for a given pitch setting. This may or may not be a problem, depending upon the fan characteristics. With direct coupling to the fan and a closed-circuit tunnel, there are no other feasible methods for achieving very low tunnel speeds if an induction motor is used to drive the fan.

Compared with a.c. motors, speed control using a d.c. motor is relatively simple. Its main advantages are that speed control is available down to zero speed and this greatly simplifies the problem of starting a system with high inertia. However, maintenance costs are high compared with induction motors. The development of compact solid-state rectifiers has increased the reliability and reduced the cost of d.c. power supplies with the result that this method of speed control is widely used in wind tunnels requiring drive motors larger than about 50 hp (37 kW.)

3.14 SUMMARY

The performance requirements for a low-speed boundary layer wind tunnel can be met with a closed-circuit design employing an over/under arrangement and a contraction ratio of 3.2:1. Recommended test section dimensions are W = 10 ft (3.048 m), H = 6 ft (1.829) and L = 55 ft (16.764 m), measured to the turntable. Because of space limitations, it is necessary to place severe restrictions on the transverse dimensions of the return section with a correspondingly low energy ratio (E.R. = 0.53).

An axial flow fan with a diameter of 8 ft (2.438 m) is recommended. Both variable pitch and variable speed will be required to ensure stable operation over the specified range of speed. Pitch control under load is not necessary and this feature can be provided by a fan hub with manually adjustable blades.

The estimated maximum power demand is based on a fan efficiency of 72 percent, approximately 4 points below peak efficiency for the fan considered here. It is anticipated that an operating efficiency in the range 75-80 percent can be achieved with proper choice of a standard production model fan. Maximum power demand will be approximately 180 hp (134 kW) and this can be reduced to 150 hp (112 kW) if the maximum tunnel speed is reduced to 75 fps (22.86 m/s).

Either an induction motor with variable frequency control or a d.c. motor with variable voltage control can be used for speed regulation. The d.c. drive system is expected to have a lower initial cost, but a higher maintenance cost.

4. OPEN-CIRCUIT TUNNEL DESIGN

4.1 GENERAL

The open-circuit tunnel arrangement shown in figure 12 should be considered as an alternative to the closed-circuit design if it is determined that a thermal modeling capability is not essential to the conduct of CBT research activities. The major advantages of this arrangement are its lower initial cost, easier access to the turntable near the end of the test section, and most important, operation of the test section at a static pressure just slightly above outside ambient pressure. Major disadvantages are a greater power demand for the same tunnel speed and a less comfortable laboratory working environment.

The open-circuit design makes use of the same settling chamber and contraction described earlier for the closed-circuit arrangement. Because of different inlet conditions and a different type of fan, a redesign of the wide-angle diffuser is required. The test section, although slightly shorter, has many of the same features proposed for the closed-circuit scheme.

4.2 WIDE-ANGLE DIFFUSER

The wide-angle diffuser for the open-circuit arrangement is shown in figure 13. Since the diffuser inlet geometry must be compatible with the discharge side

of the fan, the inlet dimensions indicated in figure 13 are based upon dimensions of a typical fan having the required capacity.

For reasons discussed later, the tunnel design assumes a centrifugal fan. An undesirable feature of this type of fan is the highly nonuniform distribution of velocity at the fan outlet. Not only is this distribution highly nonuniform, but the distribution changes significantly with fan speed. For this reason a plenum and a diffusing screen are incorporated with the diffuser inlet. As has been discussed elsewhere in this report, a screen with head loss coefficient $K = 2.8$ has been shown to be most efficient in promoting flow uniformity.

Splitter plates or vanes have been incorporated in the diffuser design to prevent transitory separation and stalling. The reason for selecting splitter plates over diffusing screens is that some provision must be made for silencing the fan and although there is room in the plenum for splitter plates, they would interfere with the redistribution of flow that must occur within the plenum.

The divergence angle for the wide-angle diffuser is 18 degrees in the vertical plane and 24 degrees in the horizontal plane. A 3 x 3 cell array formed by the splitter plates would reduce the individual divergence angles to a maximum of 8 degrees which is considered to be an upper limit for stable operation of the diffuser. However, there are two arguments for adopting a 4 x 4 cell array. First, some "fine tuning" of the splitter plates will be required to establish equal flow rates in the individual cells and this can best be accomplished with vertical and horizontal splitters located in the planes of symmetry of the diffuser. Second, the efficiency of the splitter plates as acoustic silencers will increase with increasing length to width ratio of the cells.

The head loss coefficient for the diffuser is estimated by treating the individual cells as equivalent conical diffusers with an outlet to inlet area ratio of 1.55 and a ratio of length to inlet radius of 5.33. According to the flow regime boundaries defined in reference 36, a conical diffuser with these parameters can be expected to operate with attached flow throughout the length of the diffuser. Note that the splitter plates stop short of the end of the diffuser to allow for redistribution of the flow directly ahead of the second diffusing screen.

The pressure recovery coefficient and the total-pressure loss coefficient are obtained from reference 36 based on the assumption that the settling chamber, honeycomb and screens function effectively as a tailpipe for the 16 diffuser cells. The corresponding values of these coefficients are $C_{pr} = 0.50$ and $K_t = 0.13$. In order to suppress the wakes created by the splitter plates, the head loss coefficient of the downstream diffusing screen is set at $K = 2.8$. Because of the high loss due to the diffusing screens at each end of the wide-angle diffuser, uncertainties as to the value of the total-loss coefficient for the diffuser are relatively unimportant.

4.3 TEST SECTION

The test section has the same general features as that for the closed-circuit arrangement. Because of the space required for the fan, plenum and free discharge at the end of the tunnel, the overall length of the test section is limited to 60 ft (18.288 m). A distance of 10 ft (3.048 m) has been provided between the center of the main turntable and the end of the test section for wake development and decay. This distance appears to be sufficient based on a number of boundary layer tunnels described in reference 4. If additional length is required, as may be the case for very large bluff models, a temporary extension of the floor plane can be installed.

4.4 ESTIMATION OF ENERGY RATIO

Head loss coefficients are referenced to the test-section dynamic pressure as was done for the case of the closed-circuit tunnel. These coefficients are listed in table 4 and the energy ratio is estimated to be 0.39. Compared with the energy ratio of 0.53 for the closed-circuit tunnel, the open-circuit arrangement is seen to be substantially less efficient. The major losses are due to the first diffusing screen at the juncture of the plenum and the wide-angle diffuser (35 percent) and the loss due to free discharge at the end of the test section (40 percent).

Depending upon the flow nonuniformity at the discharge side of the fan, it is possible that with proper choice of fan the head loss coefficient for the first diffusing screen can be reduced without adversely affecting the performance of the wide-angle diffuser. However there are no practical means available for reducing the loss coefficient at the end of the test section. A simple diffuser or a diffuser with turning vanes would defeat the purpose of the proposed arrangement, i.e. ease of access to the turntable and a test section static pressure close to ambient pressure. In addition, the space required for an efficient diffuser would reduce the length of the test section, already considered to be the minimum acceptable. With the proposed arrangement, a clearance of approximately 20 ft (6.10 m) has been provided between the tunnel outlet and the laboratory wall. Measurements reported in reference 30 suggest that instability of the discharge jet and a corresponding unsteadiness in the tunnel speed can result if this clearance is too small.

4.5 PRESSURE PROFILES

The total pressure and static pressure for the open-circuit tunnel operating at a speed of 80 fps (24.38 m/s) are listed in table 4 and are plotted in figure 14. The pronounced losses in total pressure due to the first diffusing screen and the free discharge are readily apparent. Exact distributions of the total and static pressure ahead of and through the fan will depend upon the shape of the fan inlet and the fan characteristics.

4.6 FAN SELECTION

As with the closed-circuit tunnel, the major criterion for choice of fan type is high capacity at relatively low total pressure head and this narrows the

selection to the axial flow and centrifugal types. If available space were not a consideration, the axial flow type would be the obvious choice because the motor and fan can be directly coupled within the fan casing and the fan discharge can be conditioned more efficiently than can that of a centrifugal fan.

However, available space is an important limitation and a substantial reduction in overall length of the tunnel can be realized by using a centrifugal fan with a double inlet. In order to simplify the transition to the settling chamber, it is desirable that the dimensions of the fan outlet be as close as possible to those of the settling chamber.

The tunnel load characteristic is plotted in figure 15 along with characteristic curves for a typical double-wheel, double-inlet, backward-bladed centrifugal fan with wheel diameter of 98 in (2.489 m). Operating points for maximum fan efficiency (82 percent) are indicated on the characteristic curves. For this particular fan, the operating efficiency will be approximately 73 percent. At maximum tunnel speed the fan speed will be about 360 rpm and the speed of the blade tips will be 154 fps (46.94 m/s). This is well below the limit of half the speed of sound recommended for low-speed tunnel applications [25].

The discussion of system stability for axial flow fans (Sec. 3.11) applies to centrifugal fans as well. Since the configuration of the fan wheel cannot be changed as can the blade pitch for an axial flow fan, it is usual to install variable-pitch vanes on the inlet bell of the fan. By adjusting the inlet vanes the flow rate can be regulated down to about 25 percent of maximum with a constant speed drive. In order to satisfy the requirement for continously variable tunnel speeds over the range of 1 to 80 fps (0.30 to 24.38 m/s), a variable speed drive will be required.

4.7 POWER REQUIREMENTS

Fan input power is plotted against tunnel speed in figure 16. The power requirement is based on a fan efficiency of 73 percent and does not account for uncertainties in estimating the energy ratio of the tunnel. Allowing a 10 percent margin for this uncertainty and for mechanical losses, the power requirement is approximately 250 hp (187 kW). For normal operation at speeds of about 40 fps (12.19 m/s) the power demand will be approximately 30 hp (22 kW).

By reducing the motor size to 200 hp (149 kW), the maximum tunnel operating speed will be approximately 75 fps (22.86 m/s), equal to that of the closed-circuit tunnel equipped with a 150 hp (112 kW) motor. The corresponding reduction in initial cost of the motor and controller is estimated to be 20 to 25 percent. Recalling that the requirement for maximum speed is based on the need to achieve critical Reynolds numbers without excessive tunnel blockage, increasing the body diameter by a factor of 8/7.5 would offset the effect of speed reduction. The corresponding solid blockage would be 5.3 vs 5.0 percent. This slight increase in solid blockage is considered acceptable in view of the cost reduction that can be realized with a 200 hp (149 kW) drive motor in the open-circuit tunnel or a 150 hp (112 kW) drive motor using a closed-circuit arrangement.

4.8 MOTOR AND CONTROLLER

Requirements for the motor and speed control system are much the same as those for the closed-circuit tunnel. A centrifugal fan allows the choice of direct coupling or belt drive, each arrangement having certain advantages and disadvantages. Because of its higher inertia, the centrifugal fan will require more attention to the design of the starting and speed control system.

4.9 SUMMARY

For applications that do not require a thermal modeling capability, an open-circuit tunnel will be adequate. A tunnel of this type can incorporate the same settling chamber, contraction and test section that have been designed for the closed-circuit arrangement. Because of minimum end clearance required for the tunnel discharge, the test section length must be reduced to 50 ft (15.240 m) as compared with 55 ft (16.764 m) for the closed-circuit arrangement.

A backward-bladed centrifugal fan with a double inlet is recommended for the open-circuit design. Because the flow on the discharge side of this type of fan is highly nonuniform, flow conditioning requires the use of diffusing screens with high head loss coefficients. This, combined with the discharge loss at the end of the tunnel, results in a relatively low energy ratio (E.R. = 0.39). For a fan operating efficiency of 73 percent the maximum power demand is approximately 250 hp (187 kW). If the maximum tunnel speed is reduced to 75 fps (22.86 m/s), a 200 hp (149 kW) motor will be adequate.

Speed regulation will require both inlet vanes and a variable speed drive to ensure stable tunnel operation at all speeds. Either an induction motor with a variable frequency controller or a d.c motor with a variable voltage controller can be used.

5. CONCLUSIONS

Based on the anticipated use of the boundary layer wind tunnel in support of research activities within the Center for Building Technology, it is concluded that tunnel operating speeds over the range of 1 to 80 fps (0.30 to 24.38 m/s) will be sufficient for a majority of applications. A turbulence intensity of approximately 0.5 percent and a maximum nonuniformity of flow on entry to the test section of $\pm$ 1 percent can be achieved using a simple honeycomb/screen combination and a contraction ratio of 3.2:1.

A test section width of 10 ft (3.048 m) and a height of 6 ft (1.829 m) will be adequate for 1:500 scale simulations of the atmospheric boundary layer and for achieving critical Reynolds numbers at or near the maximum operating speed of 80 fps (24.38 m/s). Available space limits the test section width and length. Depending on the tunnel configuration selected, test section length can range from 50 to 55 ft (15.240 to 16.764 m).

Although provisions for thermal modeling have not been considered specifically in this preliminary design effort, it is clear that such a capability will require a closed-circuit tunnel as shown in figure 1. Because of limitations

on laboratory space, an over/under arrangement is the only alternative and this will involve relatively high construction costs for the return leg of the tunnel.

If a thermal modeling capability is not considered essential to CBT research activities, the requirements for speed range and size of test section can be met with an open-circuit design as shown in figure 12. However, the power demand will be higher and the laboratory working environment will be less comfortable.

An axial flow fan with an 8 ft (2.438 m) diameter has been assumed in the design of the closed-circuit tunnel. Both variable pitch and variable speed control will be required for stable operation over the operating range of the tunnel. It is not necessary to vary the pitch while the fan is operating. For the open-circuit design a centrifugal fan with double inlet and a wheel diameter of 98 in (2.489 m) will be adequate. Adjustable inlet vanes and a variable-speed drive will be required for tunnel speed regulation.

Either an induction motor with a variable frequency controller or a d.c. motor with a variable voltage controller can satisfy the requirements for regulation of fan speed. A d.c. motor and controller are expected to have a lower initial cost, but the maintenance costs are expected to be higher than those for an induction motor with variable frequency control. Power currently available in the wind tunnel construction area consists of 480 volt 3-phase service and 120/240 volt d.c. service. The d.c. service is limited to 420 amperes which is adequate for normal tunnel operation but is insufficient to meet the maximum power demand. Therefore, a d.c. drive system must include a rectifier which is consistent with motor size. Limits on 3-phase service do not pose any problems.

Reducing the maximum tunnel speed to 75 fps (22.86 m/s) will reduce the maximum power demand from 180 hp (134 kW) to 150 hp (112 kW) in the case of the closed-circuit tunnel. Depending on the motor/controller price structure, this reduction of maximum power demand may or may not be significant. A larger reduction can be realized for the open-circuit design; 200 hp (149 kW) vs 250 hp (187 kW) and it will likely prove cost effective to limit the power demand to 200 hp (149 kW). The adverse effect of limiting tunnel speed to 75 fps (22.86 m/s) would be to increase the solid blockage from 5.0 to 5.3 percent in order to achieve critical Reynolds numbers using a smooth circular cylinder as a test body. In view of the associated cost reduction, this slight increase in solid blockage is considered acceptable.

6. REFERENCES

1. Engineering Hydraulics, (H. Rouse, Ed.), John Wiley & Sons, Inc., New York, NY., 1950, pp. 124.

2. Cermak, J. E., "Applications of Fluid Mechanics to Wind Engineering - A Freeman Scholar Lecture," Transactions of the ASME, Journal of Fluids Engineering, Vol. 97, No. 1, March, 1975, pp. 9-38.

3. Wind Tunnel Modeling for Civil Engineering Applications, (T. A. Reinhold, Ed.), Cambridge University Press, New York, NY, 1982.

4. Marshall, R. D., "Wind Tunnels Applied to Wind Engineering in Japan," Journal of Structural Engineering, ASCE, Vol. 110, No. 6, June, 1984, pp. 1203-1221

5. Vickery, B. J., "The Design and Performance of a Low-Cost Boundary Layer Wind Tunnel," Wind Effects on Structures, (H. Ishizaki and A. Chiu, Eds.), University of Tokyo Press, Tokyo, 1976, pp. 99-104.

6. Teunissen, H. W., "Validation of Boundary Layer Simulation: Some Comparisons Between Model and Full-Scale Flows," Wind Tunnel Modeling for Civil Engineering Applications, (T. A. Reinhold, Ed.), Cambridge University Press, New York, NY, 1982, pp. 217-235.

7. Britter, R., "Modeling Flow Over Complex Terrain and Implications for Determining the Extent of Adjacent Terrain to be Modeled," Wind Tunnel Modeling for Civil Engineering Applications, (T. A. Reinhold, Ed.), Cambridge University Press, New York, NY, 1982, pp. 186-196.

8. Melbourne, W. H., "Wind Tunnel Blockage Effects and Corrections," Wind Tunnel Modeling for Civil Engineering Applications, (T. A. Reinhold, Ed.), Cambridge University Press, New York, NY, 1982, pp. 197-216

9. Cermak, J. E., "Physical Modeling of the Atmospheric Boundary Layer in Long Boundary Layer Wind Tunnels," Wind Tunnel Modeling for Civil Engineering Applications (T. A. Reinhold, Ed.), Cambridge University Press, New York, NY, 1982, pp. 97-125.

10. Schlichting, H., Boundary Layer Theory, McGraw-Hill Publishing Co., Inc., New York, NY, 1960, pp. 536-537.

11. American National Standard A58.1 - 1982, "Minimum Design Loads for Buildings and Other Structures," American National Standards Institute, New York, NY, March, 1982.

12. Salter, C., "Experiments on Thin Turning Vanes, "Aeronautical Research Council R & M No. 2469, October, 1946.

13. Winter, K. G., "Comparative Tests of Thick and Thin Turning Vanes in the Royal Aircraft Establishment 4 x 3 ft Wind Tunnel," Aeronautical Research Council R & M No. 2589, August, 1947.

14. Patterson, G. N., "Note on the Design of Corners in Duct Systems," Aeronautical Research Council R & M No. 1773, 1936.

15. Engineering Sciences Data Unit, "Performance in Incompressible Flow of Plane-Walled Diffusers With Single-Plane Expansion," Data Item 74015, ESDU, London, June, 1974.

16. Schubauer, G. B. and Spangenberg, W. G., "Effect of Screens in Wide-Angle Diffusers," NACA TN 1610, July, 1948.

17. Moore, C. A. and Kline, S. J., "Some Effects of Vanes and of Turbulence in Two-Dimensional Wide-Angle Subsonic Diffusers," NACA TN 4080, June, 1958.

18. Cochran, D. L. and Kline, S. J., "Use of Short Flat Vanes for Producing Efficient Wide-Angle Two-Dimensional Subsonic Diffusers," NACA TN 4309, September, 1958.

19. Kachhara, N. L., Livesey, J. L. and Wilcox, P. L., "An Initial Approach to the Design of Very Wide Angle Axisymmetric Diffusers With Gauzes to Achieve Uniform Outlet Velocity Profiles," Transactions of the ASME, Journal of Fluids Engineering, Vol. 99, No. 2, June, 1977, pp. 357-364.

20. Dryden, H. L. and Schubauer, G. B., "The Use of Damping Screens for the Reduction of Wind-Tunnel Turbulence," Journal of the Aeronautical Sciences, Vol. 14, April, 1947, pp. 221-228.

21. Collar, A. R., "The Effect of a Gauze on the Velocity Distribution in a Uniform Duct," Aeronautical Research Council R & M No. 1867, 1939.

22. Stathopoulis, T., "Design and Fabrication of a Wind Tunnel for Building Aerodynamics," Journal of Wind Engineering and Industrial Aerodynamics, Vol. 16, No. 2, April, 1984, pp. 361-376.

23. Loehrke, R. I. and Nagib, H. M., "Control of Free-Stream Turbulence by Means of Honeycombs: A Balance Between Suppression and Generation," Transactions fo the ASME, Journal of Fluids Engineering, Vol. 98, No.3, September 1976, pp. 342-353.

24. Pope, A. and Harper, J. L., Low-Speed Wind Tunnel Testing, John Wiley & Sons, Inc., New York, NY, 1966.

25. Bradshaw, P. and Pankhurst, R. C., "The Design of Low-Speed Wind Tunnels," Progress in Aeronautical Sciences, Vol. 5, Pergamon Press, 1964, pp. 1-69.

26. Hussain, A. and Ramjee, V., "Effects of the Axisymmetric Contraction Shape on Incompressible Turbulent Flow," Transactions of the ASME, Journal of Fluids Engineering, Vol. 98, No. 1, March, 1976, pp. 58-69.

27. Ramjee, V. and Hussain, A., "Influence of the Axisymmetric Contraction Ratio on Free-Stream Turbulence," Transactions of the ASME, Journal of Fluids Engineering, Vol. 98, No. 3, September, 1976, pp. 506-515.

28. Fujii, K., Ueda, H. and Sato, S., "On the Basic Design and Construction of an Industrial Aerodynamics Wind Tunnel," Journal of Wind Engineering, No. 13, July, 1982, pp. 47-66.

29. Snyder, W. H., "The EPA Meterological Wind Tunnel - Its Design, Construction and Operating Characteristics," EPA-600/4-79-051, Environmental Sciences Research Laboratory, Research Triangle Park, NC, September, 1979.

30. Greenway, M. E. and Wood, C. J., "The Oxford University 4 m x 2 m Industrial Aerodynamics Wind Tunnel," Journal of Industrial Aerodynamics, Vol. 4, No. 1, January, 1979, pp. 43-70.

31. Morel, T. "Comprehensive Design of Axisymmertic Wind Tunnel Contractions," Transactions of the ASME, Journal of Fluids Engineering, Vol. 97, No. 1, June, 1975, pp. 225-233.

32. Morel, T., "Design of Two-Dimensional Wind Tunnel Contractions," Transactions of the ASME, Journel of Fluids Engineering, Vol. 99, No. 2, June, 1977, pp. 371-378.

33. Streeter, V. L., Fluid Mechanics, 2nd Ed., McGraw-Hill Book Co., Inc., New York, NY., 1958.

34. ASHRAE Handbook - 1981 Fundamentals, American Society of Heating, Refrigerating and Air-Conditioning Engineers, Inc., Atlanta, GA., 1982.

35. Dougherty, R. L. and Ingersoll, A. C., Fluid Mechanics, McGraw-Hill Book Co., Inc, New York, NY, 1954, pp. 191.

36. Engineering Sciences Data Unit, "Performance of Conical Diffusers in Incompressible Flow," Data Item 73024, ESDU, London, March, 1980.

37. Engineering Sciences Data Unit, "Pressure Drop in Ducts Across Round-Wire Gauzes Normal to the Flow," Data Item 72009, ESDU, London, June, 1972.

38. Engineering Sciences Data Unit, "A Guide to Fan Selection and Performance," Data Item 79037, ESDU, London, December, 1979.

Appendix I - NOTATION

A = Area; dimensionless coefficient

A_o = Area of test section

C_p = Pressure coefficient

C_{pi} = Wall pressure coefficient at inlet

C_{pr} = Static pressure recovery ratio

$\hat{C}_{pr}$ = Theoretical maximum pressure recovery ratio

C_R = Contraction ratio

D = Diameter

d = Characteristic dimension

E_o = Efficiency of diffuser/screen combination

E_o' = Diffuser efficiency

E.R. = Energy ratio

F_r = Froude number

g = Gravitational constant

H = Height of section

h = Height of model; contraction offset

I = Intensity of turbulence

K = Head-loss coefficient

K_t = Total-pressure loss coefficient

L = Length

n = Number of screens

n_o = Modal frequency

P = Static pressure

P_t = Total pressure

q = Dynamic pressure

R_e = Reynolds number

U = Velocity

U_h = Velocity at height of model

U_i = Velocity at inlet

U_o = Mean velocity in test section

U_r = Reduced velocity

U_z = Velocity at height z

U_∞ = Freestream velocity

$\tilde{U}$ = Local mean velocity

u = Departure from mean velocity in longitudinal direction

u,v,w = x,y and z components of velocity fluctuations

V = Wall velocity

X = Distance in direction of flow

Y = Ordinate of contraction wall profile

Z = Height above test section floor

α = Kinetic energy coefficient

β = Potential energy coefficient

δ = Boundary layer thickness

δ^* = Boundary layer displacement thickness

ν = Kinematic viscosity

ρ = Mass density

Table 1 Contraction Geometry and Pressure Gradient

X/L	Y/h	Area $(ft)^2$	C_p	$\frac{dC_p}{dX}^{-1}$ (ft)
0.000	1.000	192.000	0.902	0.000
0.050	0.986	189.652	0.900	0.007
0.100	0.948	183.312	0.893	0.013
0.150	0.891	174.033	0.881	0.020
0.200	0.819	162.802	0.864	0.028
0.250	0.738	150.497	0.841	0.038
0.300	0.652	137.853	0.811	0.050
0.350	0.563	125.456	0.771	0.063
0.400	0.475	113.749	0.722	0.079
0.450	0.391	103.037	0.661	0.095
0.500	0.313	93.516	0.588	0.112
0.550	0.242	85.282	0.505	0.126
0.600	0.179	78.359	0.414	0.134
0.650	0.127	72.718	0.319	0.134
0.700	0.084	68.287	0.228	0.125
0.750	0.051	64.968	0.147	0.105
0.800	0.027	62.638	0.083	0.079
0.850	0.012	61.155	0.037	0.050
0.900	0.004	60.356	0.012	0.024
0.950	0.001	60.046	0.002	0.007
1.000	0.000	60.000	0.000	0.000

1 ft = 0.3048 m

Table 2 Dimensions of Three Similar Contractions

	Wind Tunnel	Contraction Ratio	Inlet		Outlet		Length (m)	Basic Wall Profile
			Width (m)	Height (m)	Width (m)	Height (m)		
1	EPA Meteorological Wind Tunnel (Ref. 29)	2.79:1	5.490	3.960	3.660	2.130	3.350	Matched cubic arcs
2	Oxford University Industrial Aerodynamics Wind Tunnel (Ref. 30)	2.8:1	5.828	3.848	4.000	2.000	4.645	Unknown
3	NBS Boundary Layer Wind Tunnel (Proposed)	3.2:1	4.877	3.658	3.048	1.829	4.267	4th order polynomial

1 ft = 0.3048 m

Table 3. Calculation of Losses and Energy Ratio. Closed-Circuit Tunnel

Tunnel Component	K_i	A_i (sq.ft)	K_{oi}	Percent of Total Loss	Ref.	Dynamic Pressure (psf)	Loss (psf)	Total Pressure (psf)	Static Pressure (psf)
						7.296		5.264	-2.032
Test Section	0.096	60	0.096	5.08	(33)		0.700		
First Corner						7.104		4.564	0.460
Vanes	0.100	80	0.056	2.96	(13)		0.409		
Duct	0.013	80	0.007	0.37	(33)		0.051		
						4.104		4.104	0
Transition and Silencer	0.500	64	0.439	23.24	(34)		3.203		
						6.413		0.901	-5.512
Second Corner									
Vanes	0.050	64	0.044	2.33	(13)		0.321		
Duct	0.019	64	0.017	0.90	(33)		0.124		
						6.413		0.456	-5.957
Square-to-Round Transition	0.040	50.3	0.057	3.02	(35)		0.416		
						10.396		0.040	-10.356
Fan							-13.782		
						10.396		13.822	3.426
Circular Duct	0.083	50.3	0.118	6.25	(33)		0.861		
						10.396		12.961	2.565
Round-to-Square Transition	0.130	50.3	0.185	9.79	(36)		1.350		
						6.413		11.611	5.198
First Wide-Angle Diffuser	0.180	64	0.158	8.36	(15,18)		1.153		
						3.103		10.458	7.355
Third Corner									
Vanes	0.050	96	0.020	1.06	(13)		0.146		
Duct	0.016	96	0.006	0.32	(33)		0.044		
						3.103		10.268	7.165
Fourth Corner									
Vanes	0.050	96	0.020	1.06	(13)		0.146		
Duct (including entry & exit	0.019	96	0.007	0.37	(33)		0.051		
						3.103		10.071	6.968
Second Wide-Angle Diffuser									
Screen No. 1	0.700	108.7	0.213	11.28	(37)		1.554		
						2.223		8.517	6.294
Screen No. 2	0.700	148	0.115	6.09	(37)		0.839		
						1.199		7.678	6.479
Screen No. 3	0.700	192	0.068	3.60	(37)		0.496		
						0.713		7.182	6.469
Settling Chamber									
Honeycomb/Screen	1.200	192	0.117	6.19	(23,24,37)		0.854		
						0.713		6.328	5.615
Duct	0.006	192	0.006	0.32	(33)		0.044		
						0.713		6.284	5.571
Contraction	0.040	60	0.040	2.12	(35)		0.292		
						7.296		5.992	-1.304
Bluff Body in Test Section	0.100	60	0.100	5.29	(34)		0.730		
			$\sum$=1.889	$\sum$=100.00		7.296		5.262	-2.034

Notes: 1 1 ft = 0.3048 m

2. Pressures are based on U_o = 80 fps

3. 1 psf = 47.88 Pa

E.R. = $1/\sum K_{oi}$ = 0.53

Table 4. Calculation of Losses and Energy Ratio. Open-Circuit Tunnel

Tunnel Component	K_i	A_i (sq.ft)	K_{oi}	Percent of Total Loss	Ref.	Dynamic Pressure (psf)	Loss (psf)	Total Pressure (psf)	Static Pressure (psf)
						0		0	0
Fan	-	-	-	-			-18.751		
						2.610		18.751	16.141
Plenum	-	100.3	-	-			0		
						2.369		18.751	16.382
First Diffusing Screen	2.800	105.3	0.909	35.38	(37)		6.631		
						2.369		12.120	9.751
Wide-Angle Diffuser	0.130	105.3	0.042	1.63	(36)		0.306		
						0.713		11.814	11.101
Second Diffusing Screen	2.800	192	0.273	10.62	(37)		1.992		
						0.713		9.822	9.109
Settling Chamber									
Honeycomb/Screen	1.200	192	0.117	4.55	(23,24,37)		0.854		
						0.713		8.968	8.255
Duct	0.006	192	0.006	0.23	(33)		0.044		
						0.713		8.924	8.211
Contraction	0.040	60	0.040	1.56	(35)		0.292		
						7.296		8.632	1.336
Test Section									
Bluff Body	0.100	60	0.100	3.89	(34)		0.730		
						7.296		7.902	0.606
Duct	0.083	60	0.083	3.23	(33)		0.606		
						7.296		7.296	0
Discharge	1.000	60	1.000	38.91			7.296		
			$\sum$=2.570	$\sum$ = 100.00		0		0	0

$$E.R. = 1/\sum K_{oi} = 0.39$$

Notes: 1. 1 ft = 0.3048 m
2. Pressures are based on U_o = 80 fps
3. 1 psf ≈ 47.88 Pa

1	Test Section	9	First Wide-Angle Diffuser
2	First Corner	10	Third Corner
3	Acoustic Silencer	11	Vertical Duct
4	Second Corner	12	Fourth Corner
5	Square-to-Round Transition	13	Second Wide-Angle Diffuser
6	Drive Section	14	Settling Chamber
7	Return Duct	15	Contraction
8	Round-to-Square Transition		

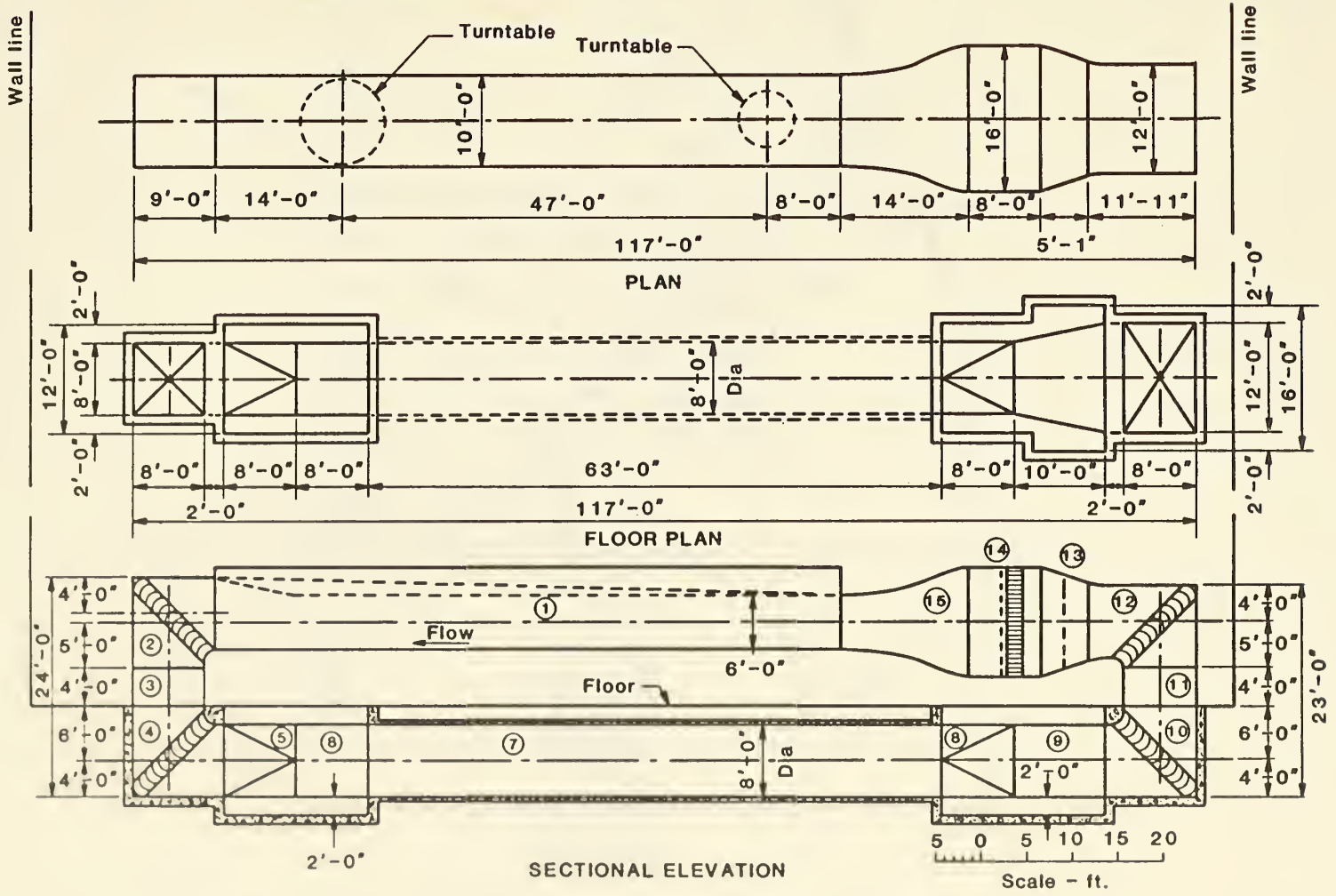

Figure 1. Closed-Circuit Tunnel. Plan and Sectional Elevation

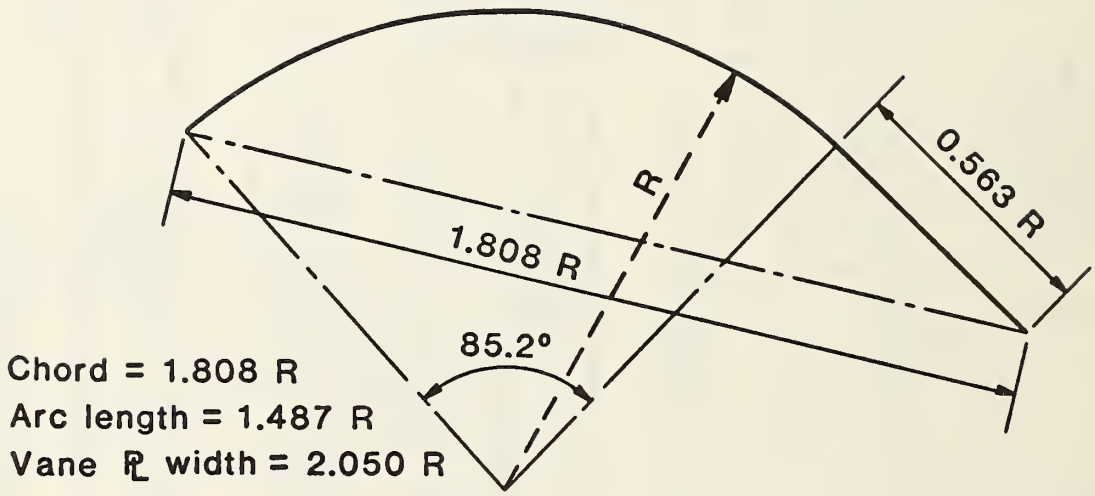

Figure 2. Turning Vane Profile. Closed-Circuit Tunnel

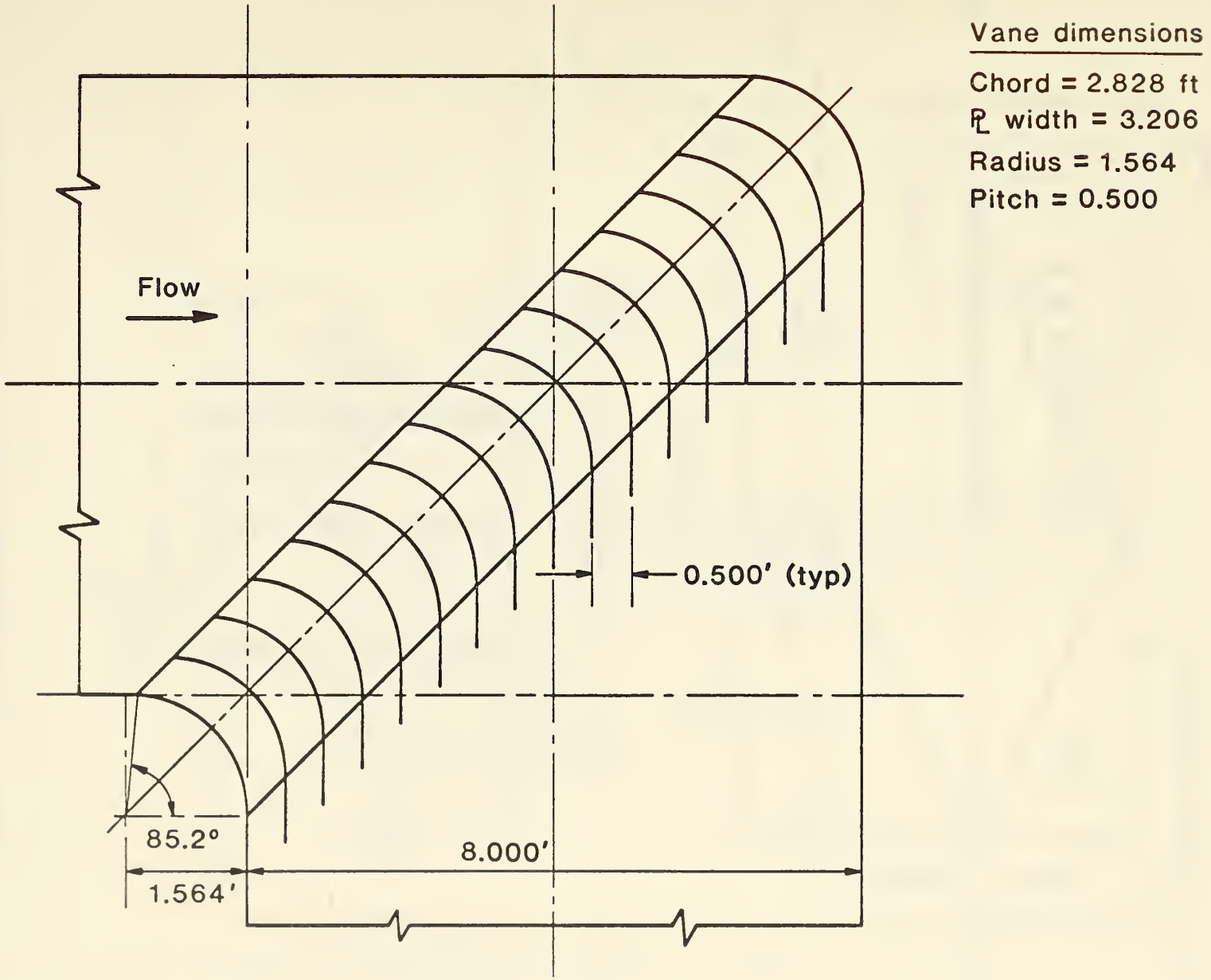

Figure 3. Typical Vane Cascade. Closed-Circuit Tunnel

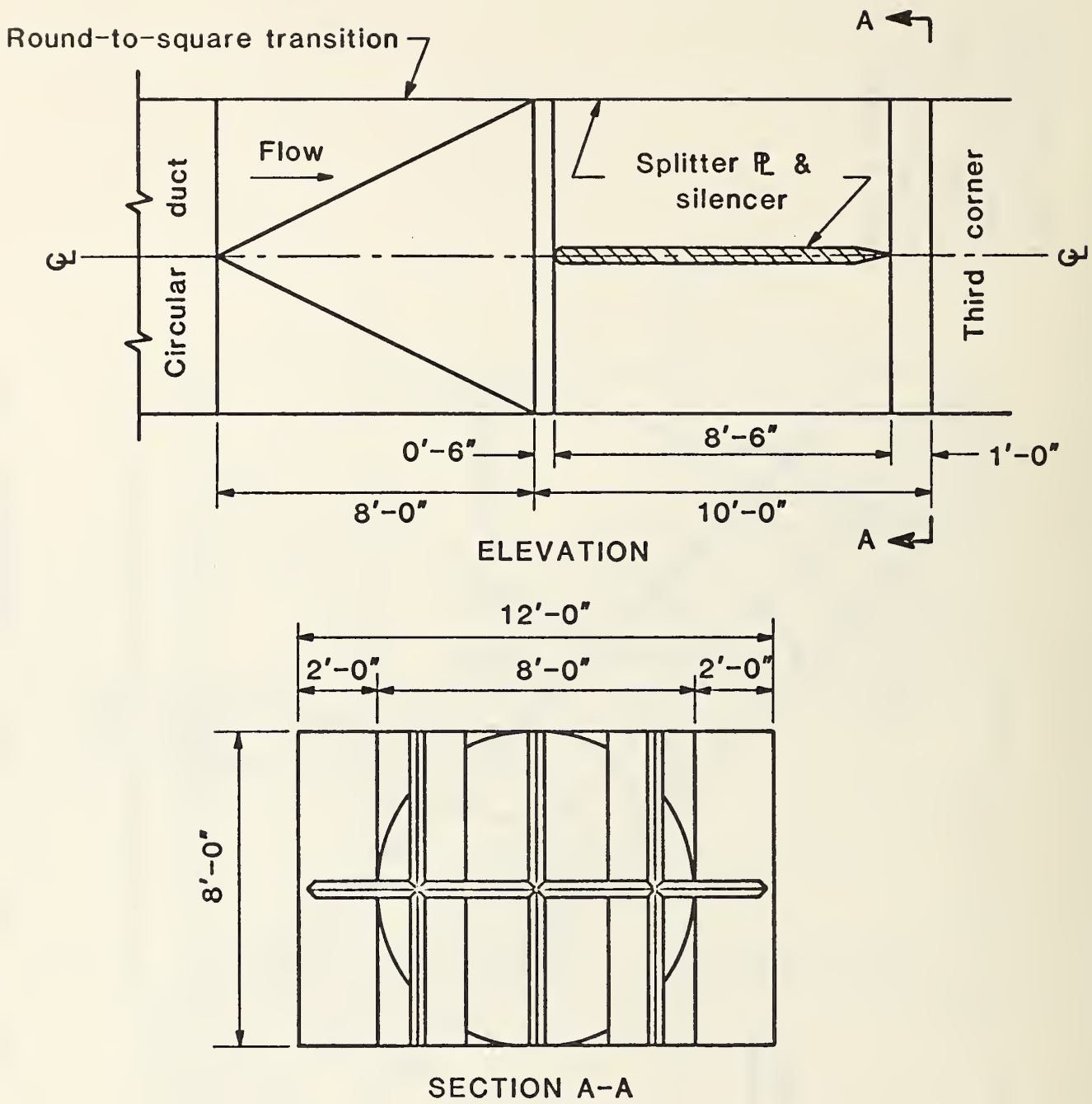

Figure 4. First Wide-Angle Diffuser. Closed-Circuit Tunnel

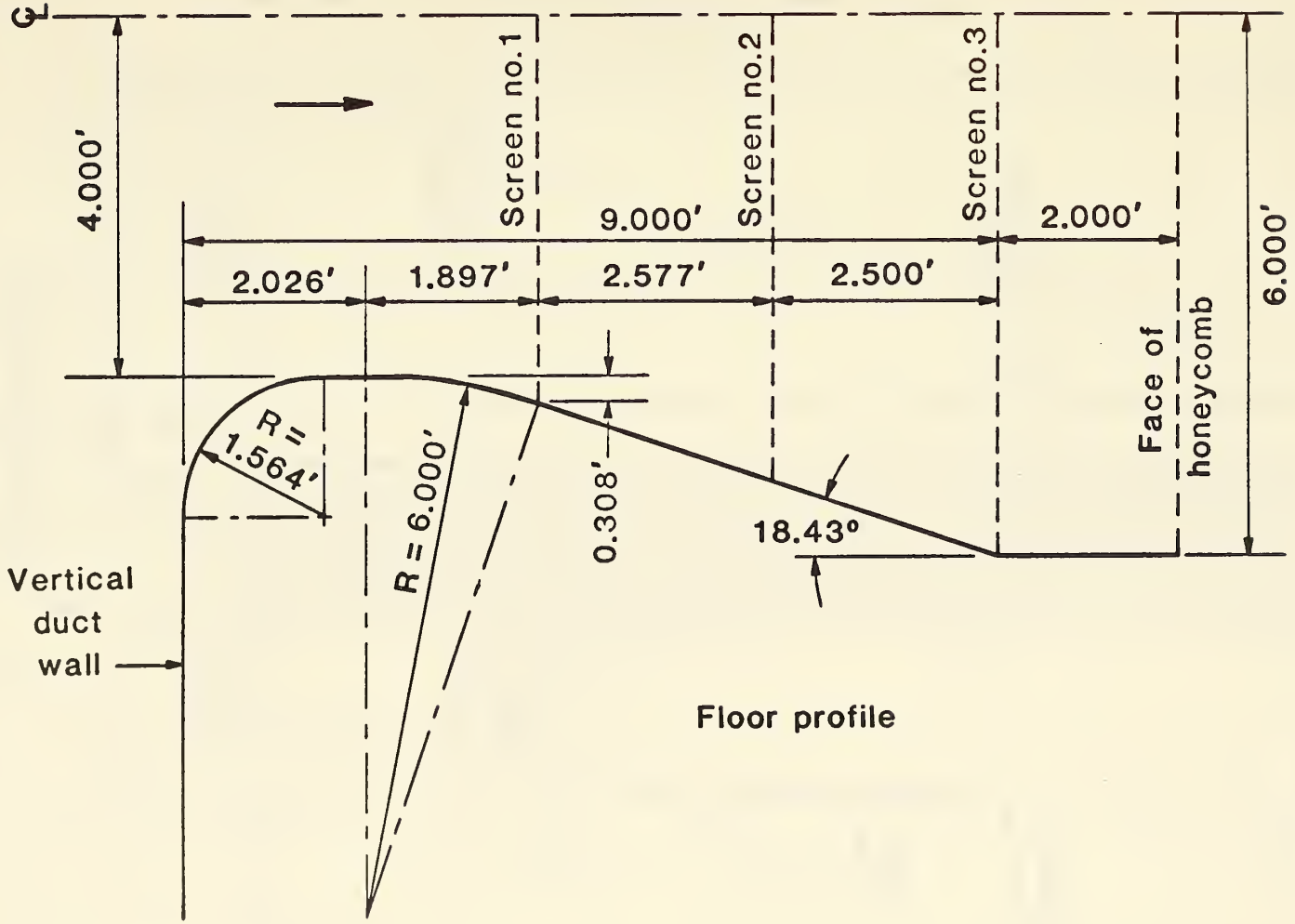

Figure 5. Second Wide-Angle Diffuser. Closed-Circuit Tunnel

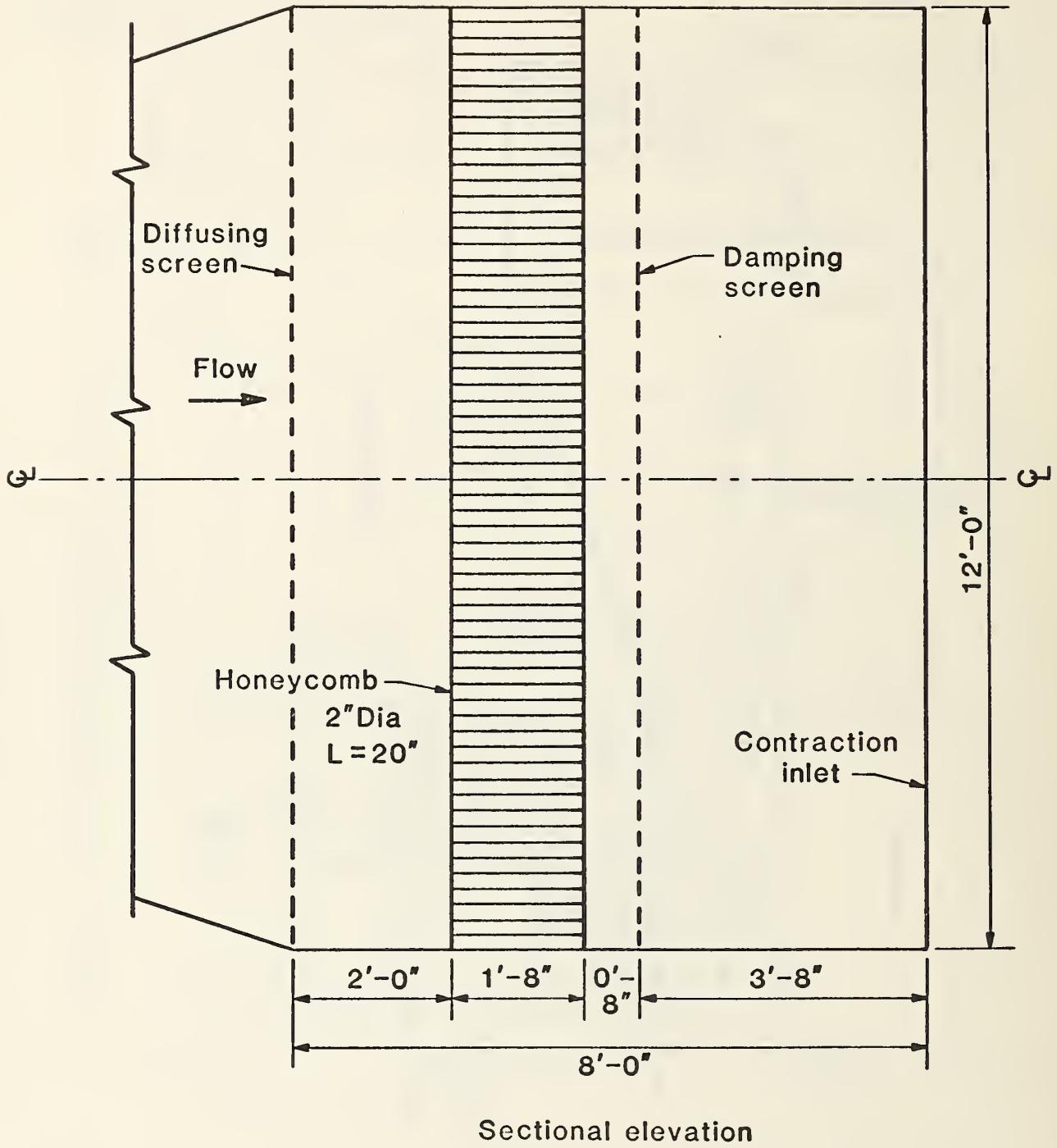

Figure 6. Settling Chamber

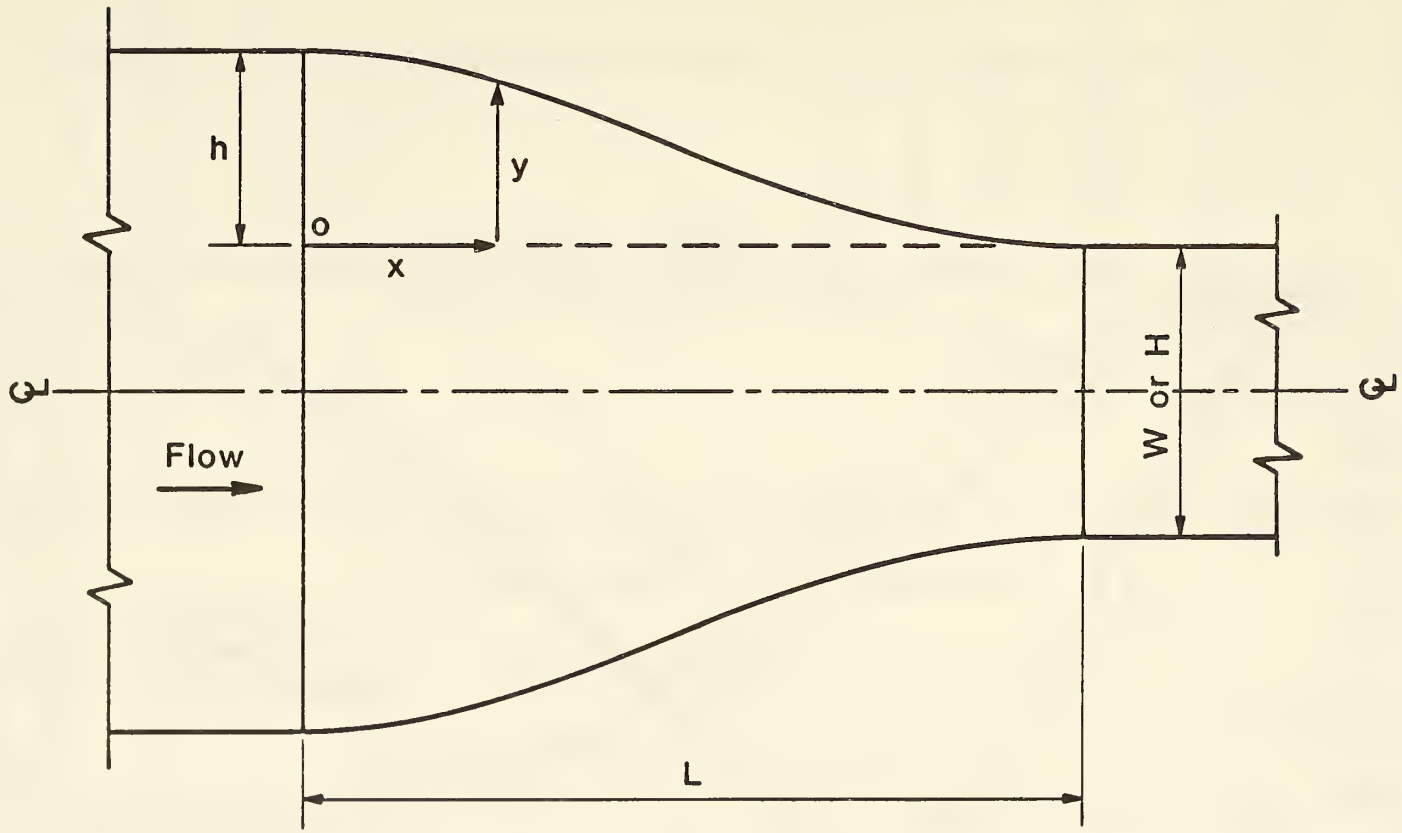

Figure 7. Contraction Profile. Definition Sketch

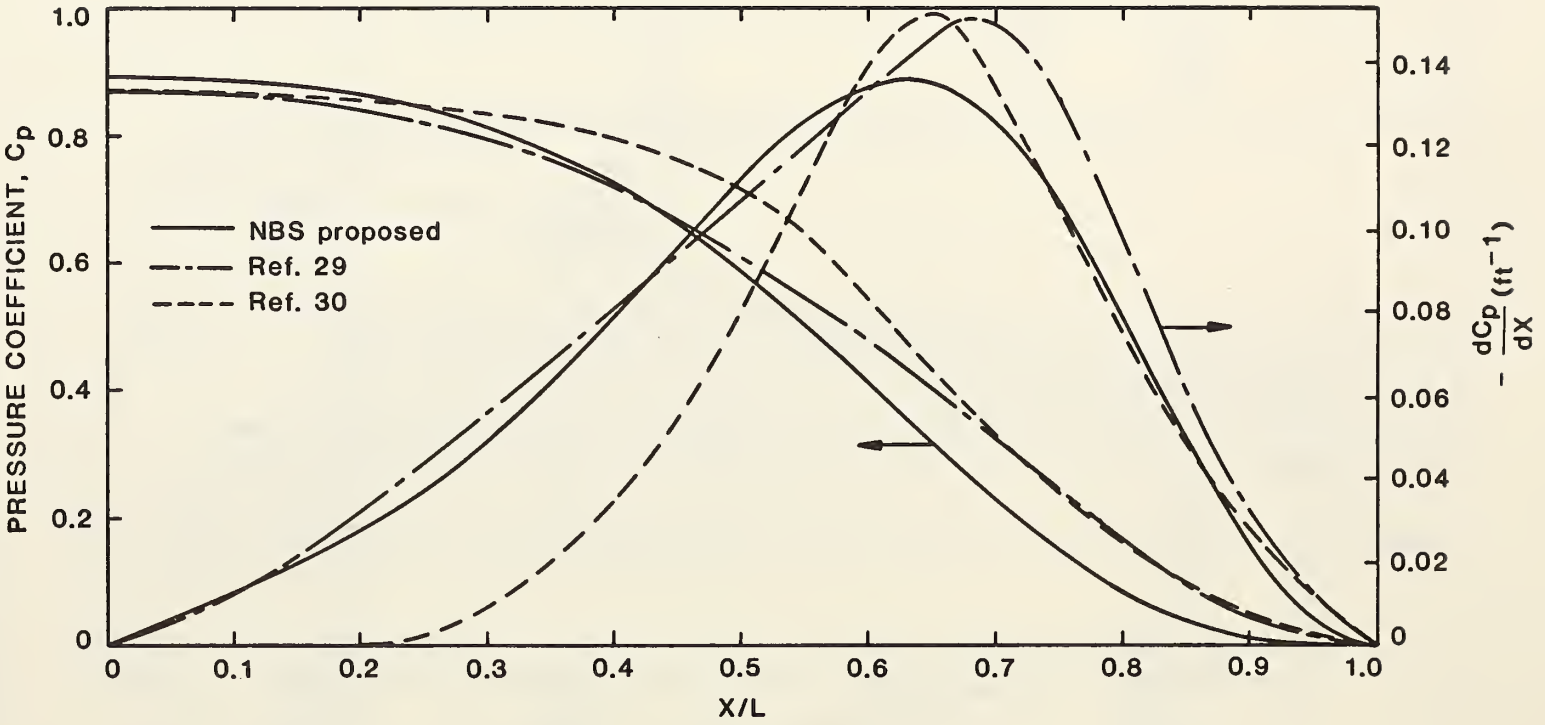

Figure 8. Pressure Coefficient and Gradient for Three Similar Contractions

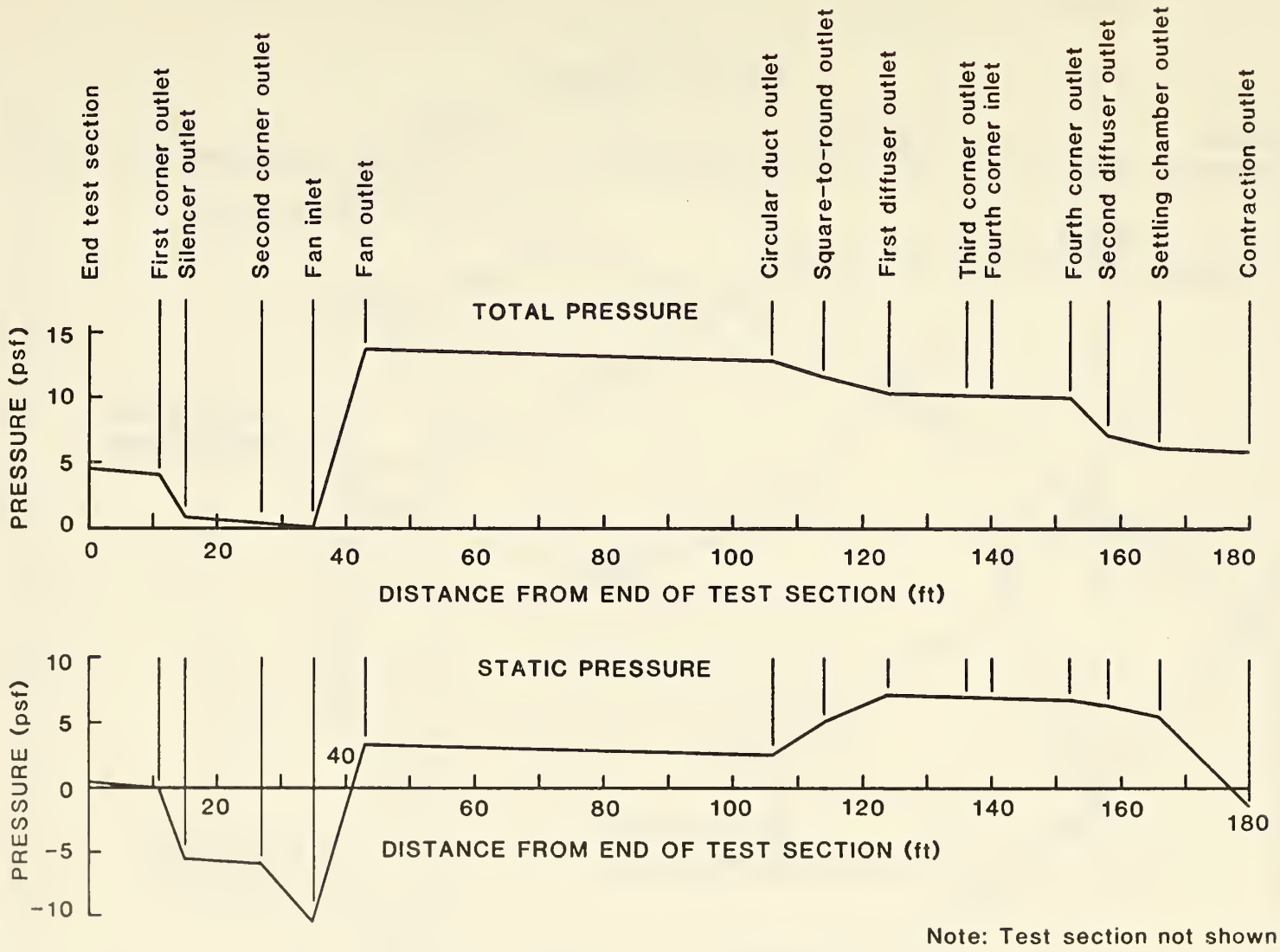

Figure 9. Pressure Profiles. Closed-Circuit Tunnel. (U_o = 80 fps)

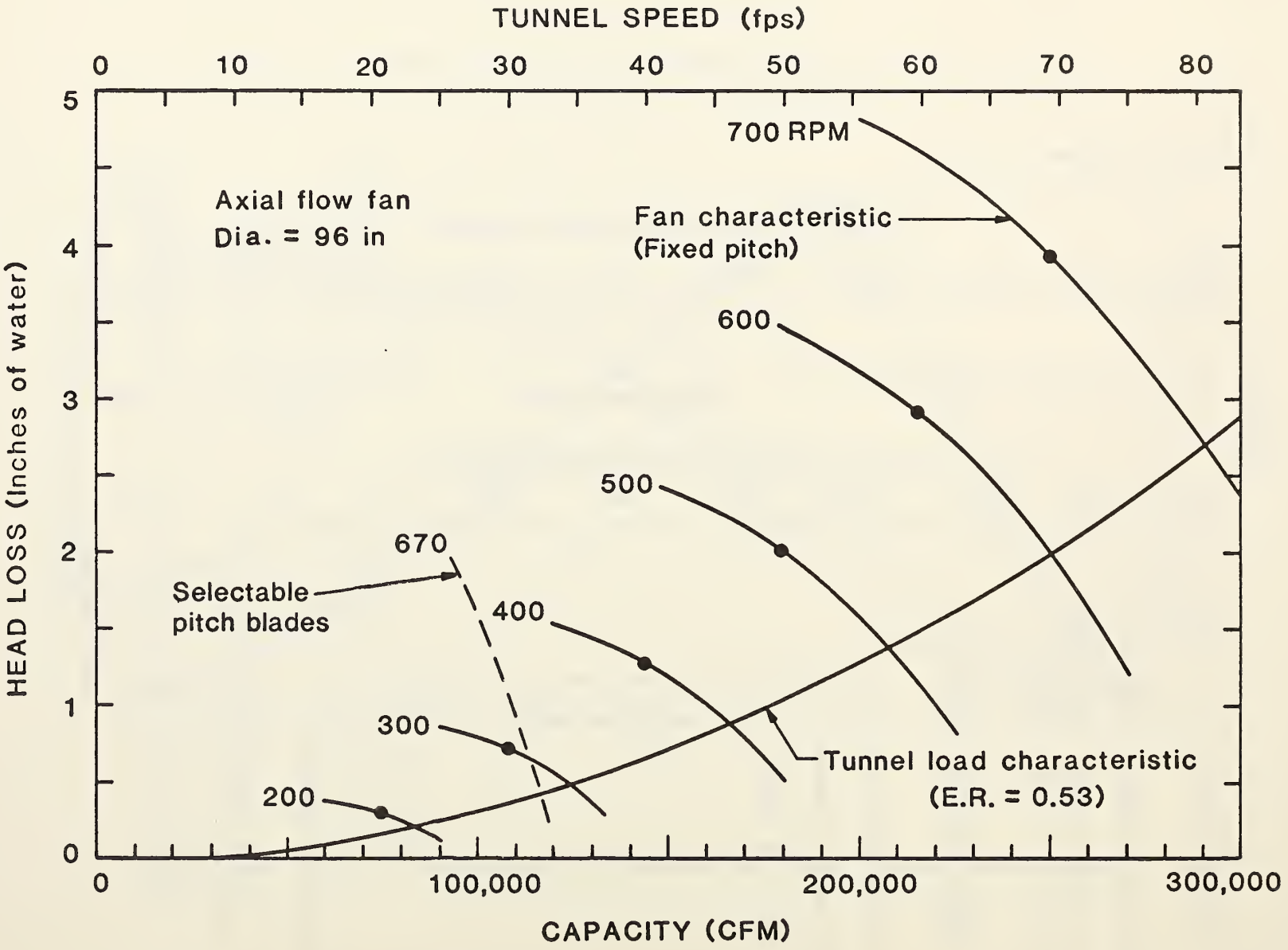

Figure 10. Tunnel and Fan Characteristics. Closed-Circuit Tunnel

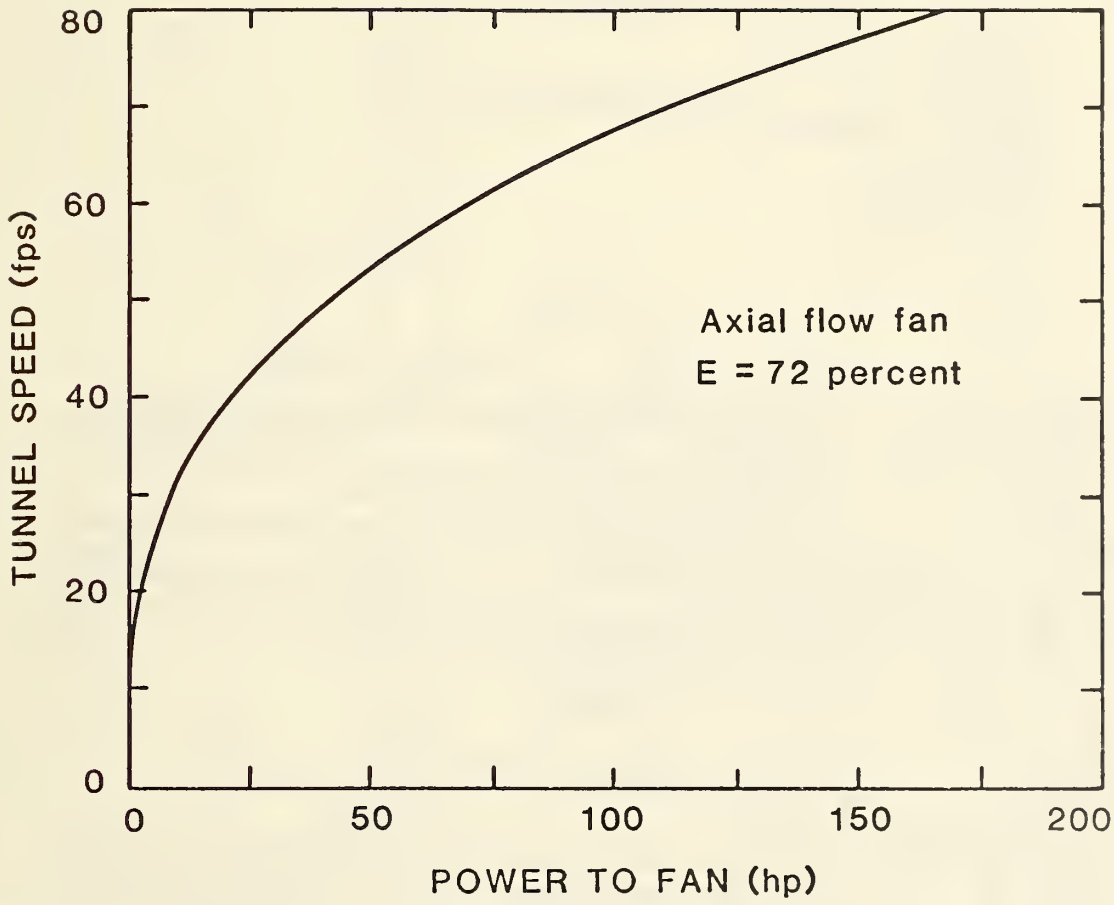

Figure 11. Power Demand Curve. Closed-Circuit Tunnel

1 Centrifugal Fan

2 Plenum

3 Wide-Angle Diffuser

4 Settling Chamber

5 Contraction

6 Test Section

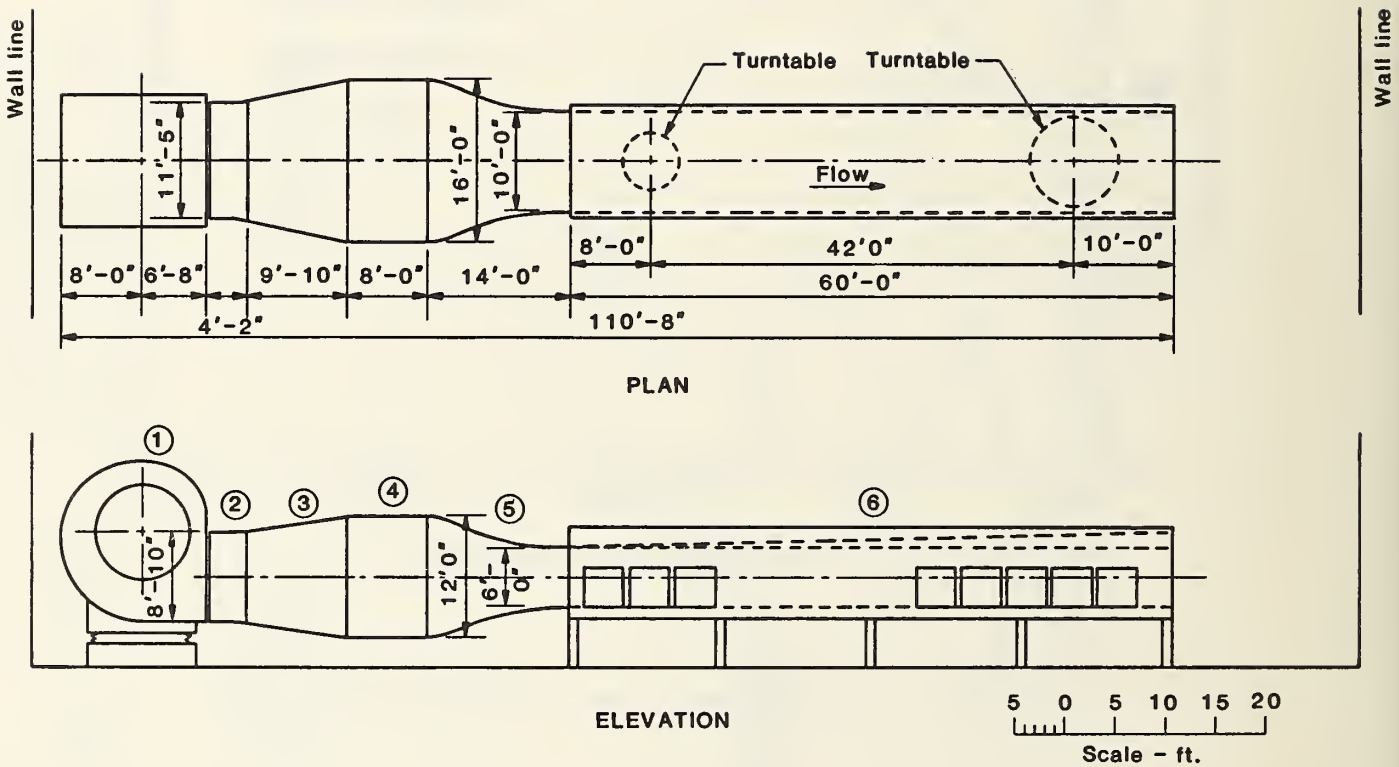

Figure 12. Open-Circuit Tunnel. Plan and Elevation

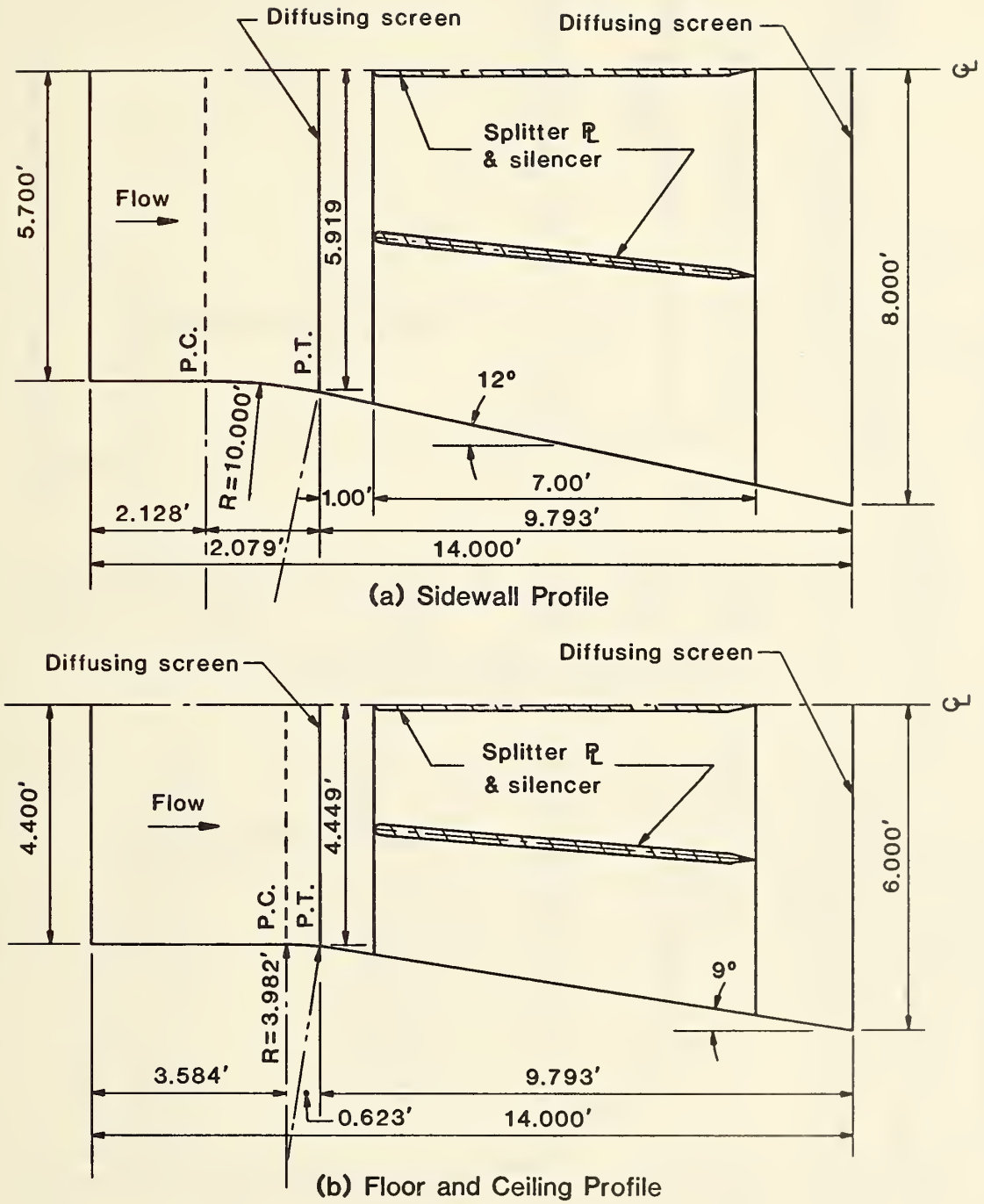

Figure 13. Wide-Angle Diffuser. Open-Circuit Tunnel

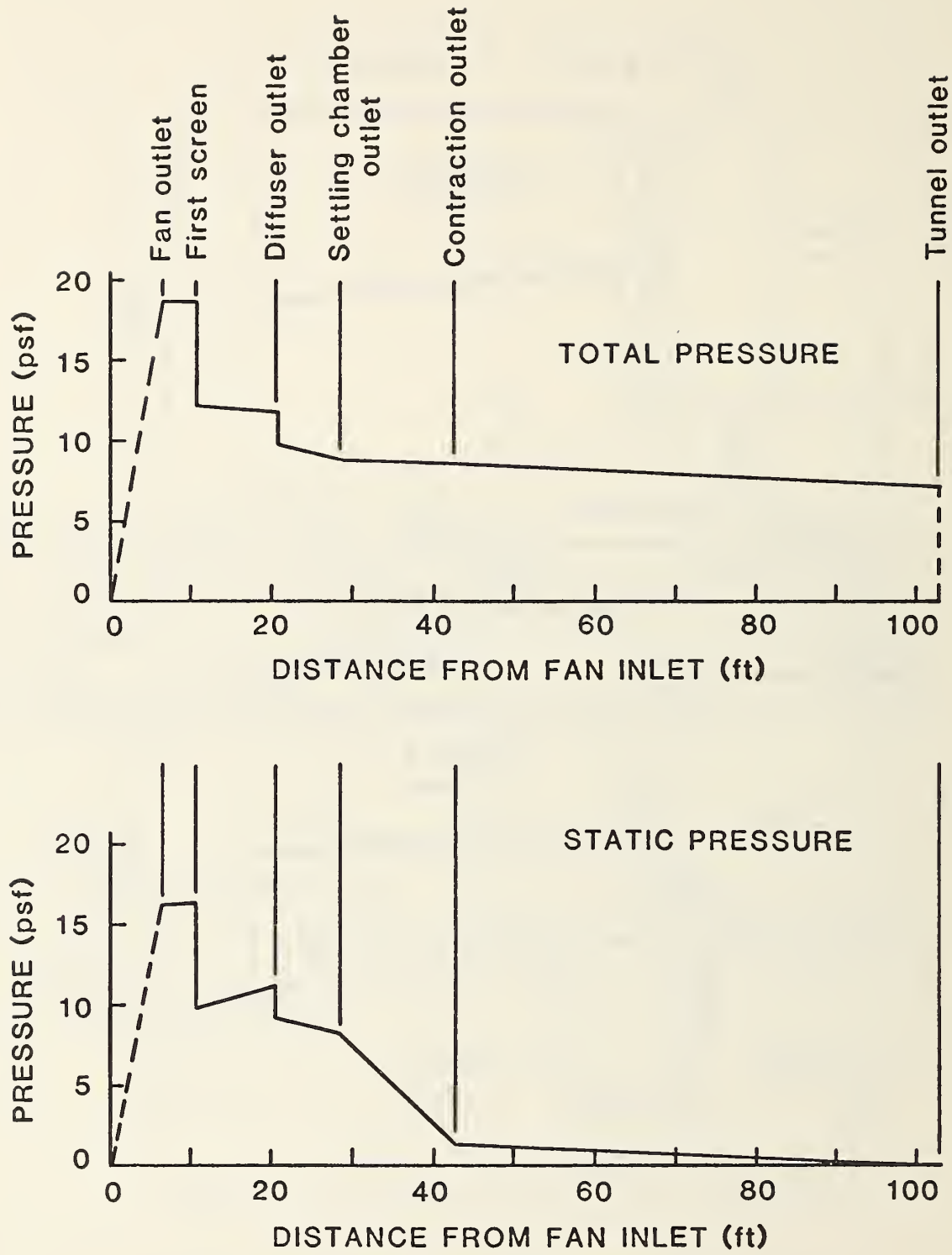

Figure 14. Pressure Profiles. Open-Circuit Tunnel. (U_o = 80 fps)

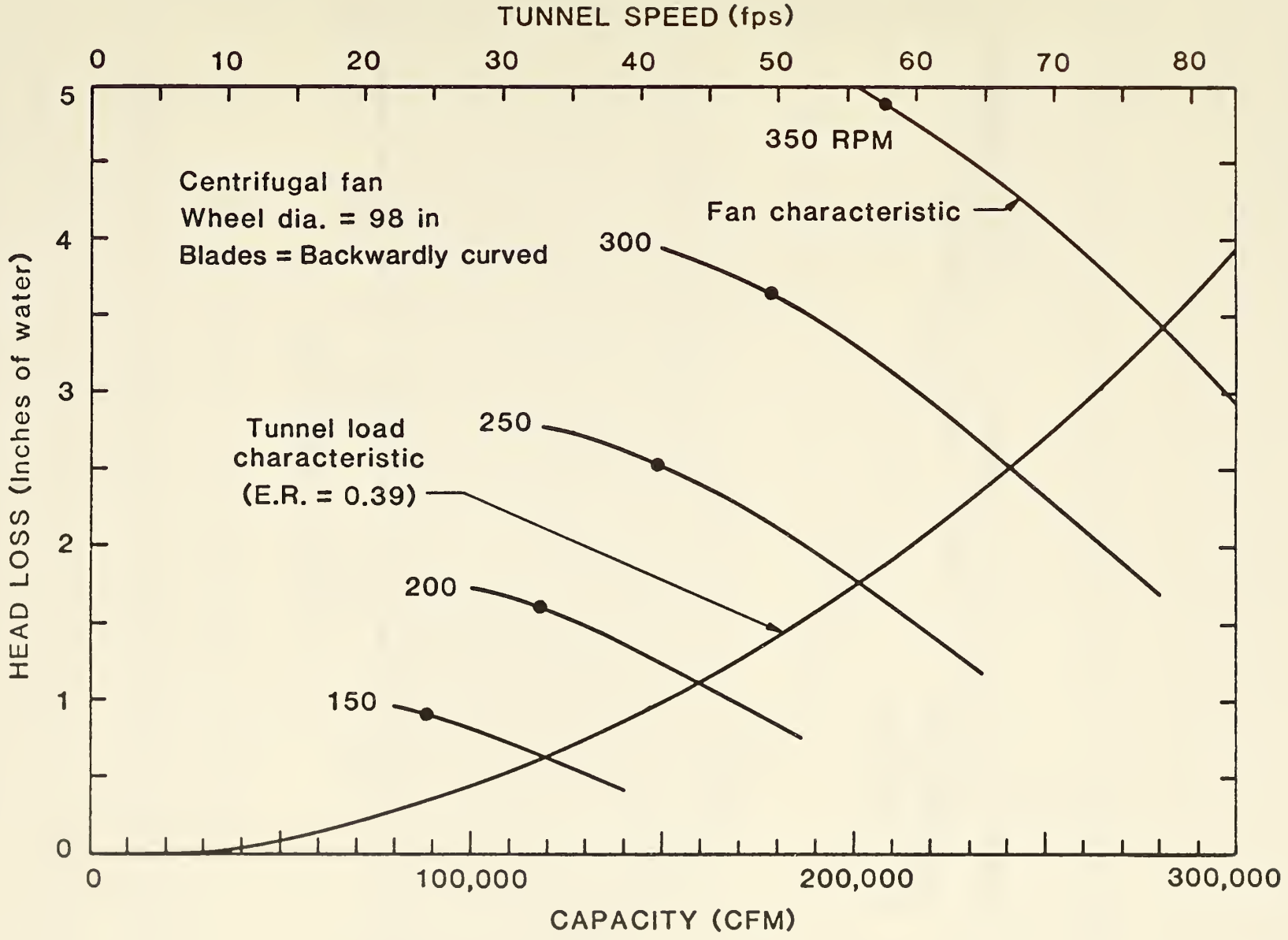

Figure 15. Tunnel and Fan Characteristics. Open-Circuit Tunnel

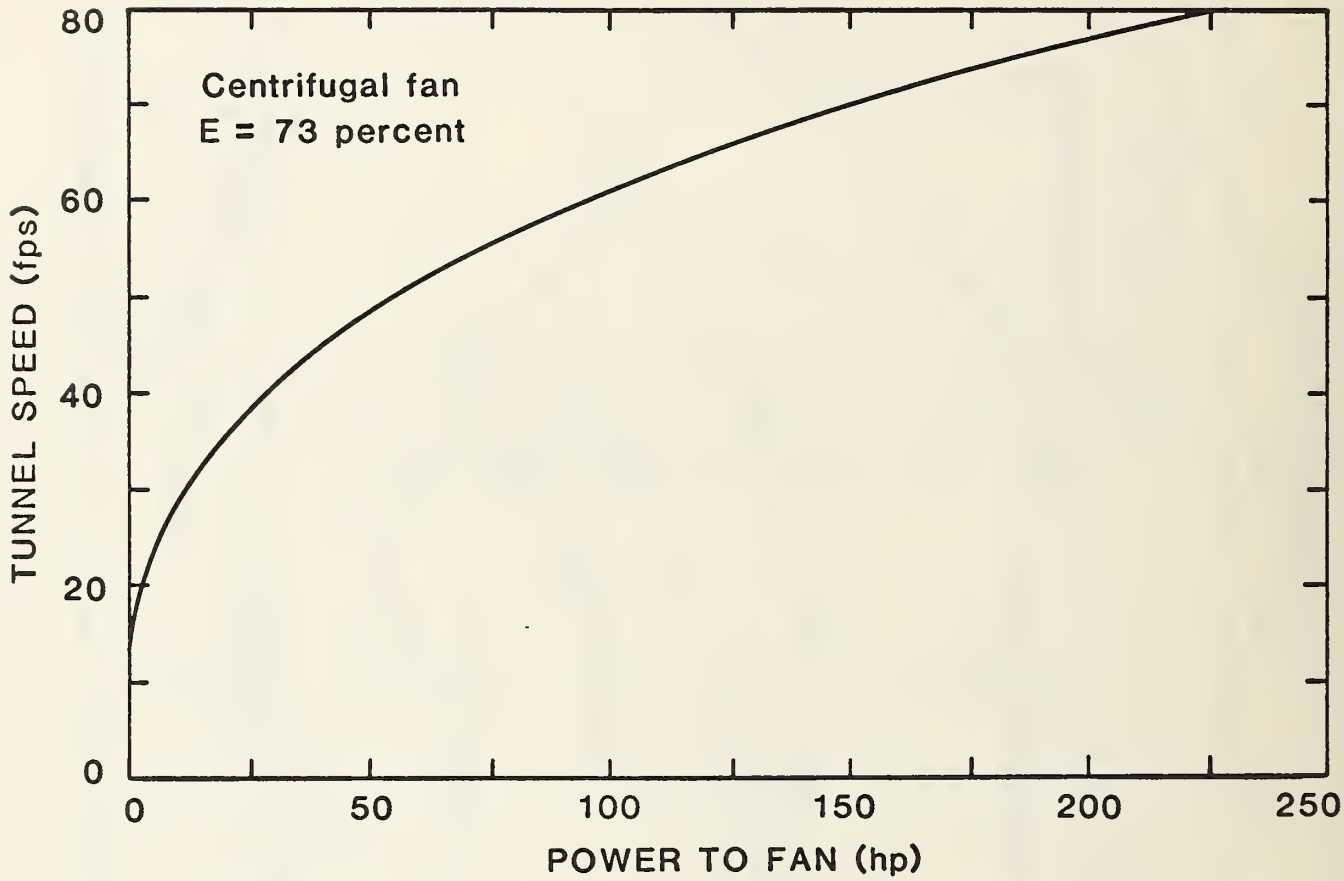

Figure 16. Power Demand Curve. Open-Circuit Tunnel

NBS-114A (REV. 2-8C)

U.S. DEPT. OF COMM. BIBLIOGRAPHIC DATA SHEET (See instructions)	1. PUBLICATION OR REPORT NO. NBSIR 85-3168	2. Performing Organ. Report No.	3. Publication Date May 1985

4. TITLE AND SUBTITLE

Performance Requirements and Preliminary Design of a Boundary Layer Wind Tunnel Facility

5. AUTHOR(S)

Richard D. Marshall

6. PERFORMING ORGANIZATION (If joint or other than NBS, see instructions)

NATIONAL BUREAU OF STANDARDS
DEPARTMENT OF COMMERCE
~~WASHINGTON, D.C. 20234~~
Gaithersburg, MD 20899

7. Contract/Grant No.

8. Type of Report & Period Covered

Final

9. SPONSORING ORGANIZATION NAME AND COMPLETE ADDRESS (Street, City, State, ZIP)

same as item 6 above

10. SUPPLEMENTARY NOTES

☐ Document describes a computer program; SF-185, FIPS Software Summary, is attached.

11. ABSTRACT (A 200-word or less factual summary of most significant information. If document includes a significant bibliography or literature survey, mention it here)

This report describes performance characteristics and design details of a boundary layer wind tunnel for supporting research activities within the Center for Building Technology. Two preliminary designs, the first consisting of a conventional closed-circuit scheme in an over/under configuration and the second consisting of an open-circuit scheme with a "pusher" or "blow-down" configuration, are addressed. Both tunnels incorporate a three-dimensional contraction with a 3.2:1 contraction ratio and a test section having a width of 10 ft (3.048 m) and a height of 6 ft (1.829 m). The test section length allows for the natural development of rough-wall boundary layers of sufficient depth for 1:500 scale simulations of the atmospheric boundary layer. To ensure stable operation over the design speed range of 1 to 75 fps (0.30 to 22.86 m/s), both variable pitch and variable speed fan control will be required.

12. KEY WORDS (Six to twelve entries; alphabetical order; capitalize only proper names; and separate key words by semicolons)

Aerodynamics; boundary layers; buildings; modeling; wind engineering; wind tunnels.

13. AVAILABILITY

☒ Unlimited

☐ For Official Distribution. Do Not Release to NTIS

☐ Order From Superintendent of Documents, U.S. Government Printing Office, Washington, D.C. 20402.

☒ Order From National Technical Information Service (NTIS), Springfield, VA. 22161

14. NO. OF PRINTED PAGES

67

15. Price

$10.00

USCOMM-DC 6043-P80